

# Geoelectric Model of the Central Part of the Northern Caucasus and Its Fluid Saturation

V. V. Belyavsky\*

*Geoelectromagnetic Research Center, Schmidt Institute of Physics of the Earth, Russian Academy of Sciences, Troitsk, Moscow, 108840 Russia*

*\*e-mail: victor.belyavsky@list.ru*

Received July 12, 2022; revised December 12, 2022; accepted December 20, 2022

**Abstract**—A series of magnetotelluric and seismic studies have been carried out on profiles covering more than two thousand kilometers within the North Caucasus region. The earlier interpretation of the magnetotelluric observations by means of one- and two-dimensional inversion and three-dimensional mathematical modeling software has helped to construct a series of sections and models which are viewed as test and starting ones for the construction of a three-dimensional geoelectric model of the region. The test models have been used to test how well the software for three-dimensional inversion of the impedance tensor components in the magnetotelluric sounding method can estimate the parameters of conducting blocks in the structures of the Greater Caucasus and the Scythian plate. In the resulting geoelectric model, constructed from the results of three-dimensional inversion of all impedance tensor components, the position of low-resistance blocks correlates with deep faults, volcanoes of various genesis, and seismically active zones characterized by the reduced velocity of seismic waves and their increased absorption. The electrical resistivity of low-resistance anomalies is explained by the degree of their saturation with the fluid water fraction. Its maximum concentration is found within the intersections of fault systems, flexural-rupture zones, and deep faults activated by tectonic processes.

**Keywords:** electrical conductivity, magnetotelluric sounding, geoelectric sections, fluid saturation

**DOI:** 10.1134/S1069351323040018

## INTRODUCTION

The regional magnetotelluric studies conducted in the North Caucasus region were aimed at studying the deep structure of lithospheric plates and volcanic systems of various genesis, the conditions under which mineral deposits are formed and seismic processes are activated. The magnetotelluric studies were used to construct geoelectric models of the sedimentary cover, folded basement and crystalline basement of the Ciscaucasian part of the Scythian plate, folded structures of the Greater Caucasus, volcanic chambers of the Elbrus volcano and the Taman trough, and to estimate their saturation with the fluid water fraction.

Magnetotelluric soundings (MTS) in the central part of the North Caucasus were performed in the range of periods  $0.01 < T < 1000$  s by means of CES-2, CES-M and Phoenix stations with 1–5 km intervals between observation points (o.p.) by Electromagnetic Research Center LLC, Severo-Zapad LLC, and Kavkazgeolsyemka Association. The presented results of the magnetotelluric (MT) studies took into account one- and two-dimensional inversions of the MTS curves (Shempelev et al., 2020; 2005). Studies performed with three-dimensional (3D) test models

showed that the interpretation of profile magnetotelluric observations based on one- or two-dimensional inversions often leads to false structures, while their three-dimensional inversion gives a more realistic representation of 3D structures and under a single observation profile (Siripunvaraporn et al., 2005; Ivanov and Pushkarev, 2012; Kiyan et al., 2014). These and several other papers show that it is necessary to include additional impedances  $Z_{xx}$  and  $Z_{yy}$  in the MT data inversion process when the impedance tensors are three-dimensional.

The test 3D model constructed for the North Caucasus region by interactively fitting the 3D model  $\rho_m(T)$  to the experimental  $\rho_{ob}(T)$  curves calculated with the 3D modeling software Maxwellf (Druskin and Knizhnerman, 1994) was used to evaluate the ability of the 3D inversion software WSINV3DMT (Siripunvaraporn et al., 2004) to restore its geoelectric parameters. When performing a three-dimensional inversion, we need to specify the starting models. The upper part of these models was based on 1D/2D inversions of the invariant MTS curves, while the lower part was based on the data and 3D modeling of the MT fields. Testing the WSINV3DMT software showed

that it significantly corrects the parameters of conducting blocks in the folded basement and fault zones of its secants presented earlier by (Belyavsky, 2007).

The observations on the MTS profiles carried out by Kavkazgeolsyemka Association and GEON Center using the earthquake converted wave (ECWM) and deep seismic sounding (DSS) methods (Belyavskii et al., 2006), combined with the three-dimensional inversion of the MT data carried out in the eastern and western parts of the North Caucasus region helped to estimate the content of bound portions of the fluid water fraction in the crust of the Greater Caucasus, the Scythian plate, the Taman and Terek–Caspian troughs.

### OVERVIEW OF THE NORTH CAUCASUS STRUCTURE

The current structure of the North Caucasus region (Fig. 1) includes (*Atlas...*, 1998; Voblikov and Lopatin, 2002):

- the folded system of the Greater Caucasus, which has the Main Range anticlinorium and the North Caucasus marginal massif in the central part of the mountains, the Novorossiysk folded zone in the west, and the Limestone Dagestan overthrust, the Agvali monocline, the Lateral Range and Main Range anticlinoriums of the Eastern Caucasus, the zones of near–edge and near–axis folds in the east;

- the zone of the Ciscaucasian marginal troughs deposited on the Scythian Epi–Hercynian plate and filled with Neogene–Quaternary molasse. In the west, it is the periclinal Taman trough, which merges into the Indol–Kuban trough, and in the east, it is the Terek–Caspian trough. According to the ECWM data, the structures of the Northwest Caucasus within the Novorossiysk folded zone are thrust under the Scythian plate (Zolotov et al., 2001) with an amplitude of up to 10 km;

- The Scythian Epi–Hercynian plate of Ciscaucasia, consisting of the Azov–Kuban, Terek–Kuma depressions and the Stavropol arch separating them. The deformed margin of the Scythian plate is separated from the Greater Caucasus orogen along the Akhtyr fault, the Cherkessk fault, the Nalchik–Mineralnye Vody flexural–rupture zone, and the Northern overthrust of the Eastern Caucasus (Belov et al., 1990).

The pre–Hercynian basement sinks within the depressions, the Indol–Kuban and Terek–Caspian troughs sink to depths of 10–12 km (Fig. 1), and the folded basement (pre–Jurassic) sinks to depths of 6–10 km. Their internal structure and external contours generally follow the structural layout of the pre–Jurassic basement and are closely related to the structures of the North Caucasus region.

The Alpine folded zones include: the Novorossiysk and the Taman structures in the west, Limestone Dagestan in the east, and the North Caucasus marginal massif in the center, which, together with the Stavropol arch, is separated from the Terek–Caspian trough along the Nalchik–Mineralnye Vody zone with an amplitude of up to 10 km. In the east, the folded–block uplift of the Eastern Caucasus includes anticlinoriums of the Lateral Range and the Main Range, the zones of near–edge and near–axis folds (Fig. 1). It is supposed that Limestone Dagestan is thrust over Meso–Cenozoic sediments of the Terek–Caspian marginal trough with an amplitude of more than 40 km (Shatsky overthrust) (Belov et al., 1990). The allochthon of Limestone Dagestan is in its turn overlain by the Oligocene–Miocene sediments of the Terek–Caspian trough, which sink to a depth of five kilometers to the north, and the Mesozoic sediments of the sedimentary cover sink to the south (Magomedov, 2010).

The North Caucasus structures were formed under compression, which was present at all stages of the region’s development due to the interaction of the Scythian and the Transcaucasian lithospheric plates. The key phases in the development of the region are considered to be the Pre–Jurassic–Jurassic, when the Eurasian plate faulted and the Scythian and the Transcaucasian plates formed and later pressed against each other in the Late Alpine (Lukk and Shevchenko, 2019), giving rise to the nappe–folded structures of the Greater Caucasus.

#### *Central Part of the North Caucasus*

The Main Range zone of the Central Caucasus is a deeply eroded outcrop of the pre–Alpine basement, which consists of northwest–trending blocks of Proterozoic and Paleozoic metamorphic rocks, granites, shales and sandstones. The North Caucasian marginal massif is bounded by: the Main Range in the south, through the 2–12 km wide Tyrnyauz suture zone (Tyrnyauz deep fault), composed of Paleozoic volcanogenic–sedimentary deposits (Fig. 1), and the Scythian plate in the north, through the Armavir–Nevinnomyssk, Cherkessk, and Akhtyr faults, the Mineralnye Vody and the Naguta–Lysaya Gora fault–slip systems. The latter two bound the northwest–trending Nalchik–Mineralnye Vody flexural–rupture zone and cross the Elbrus–Mineralnye Vody zone of northeast–trending wrench faults (Milanovsii et al., 1989).

The marginal faults are mostly uplifts, tilted (75°–85°) north or south by the mixer planes with vertical displacement amplitudes of up to 3–4 km. The linear folds, nappes and fault structures developed within the Greater Caucasus meganticlinorium are associated with a tectonic process—the Scythian plate thrusting over the

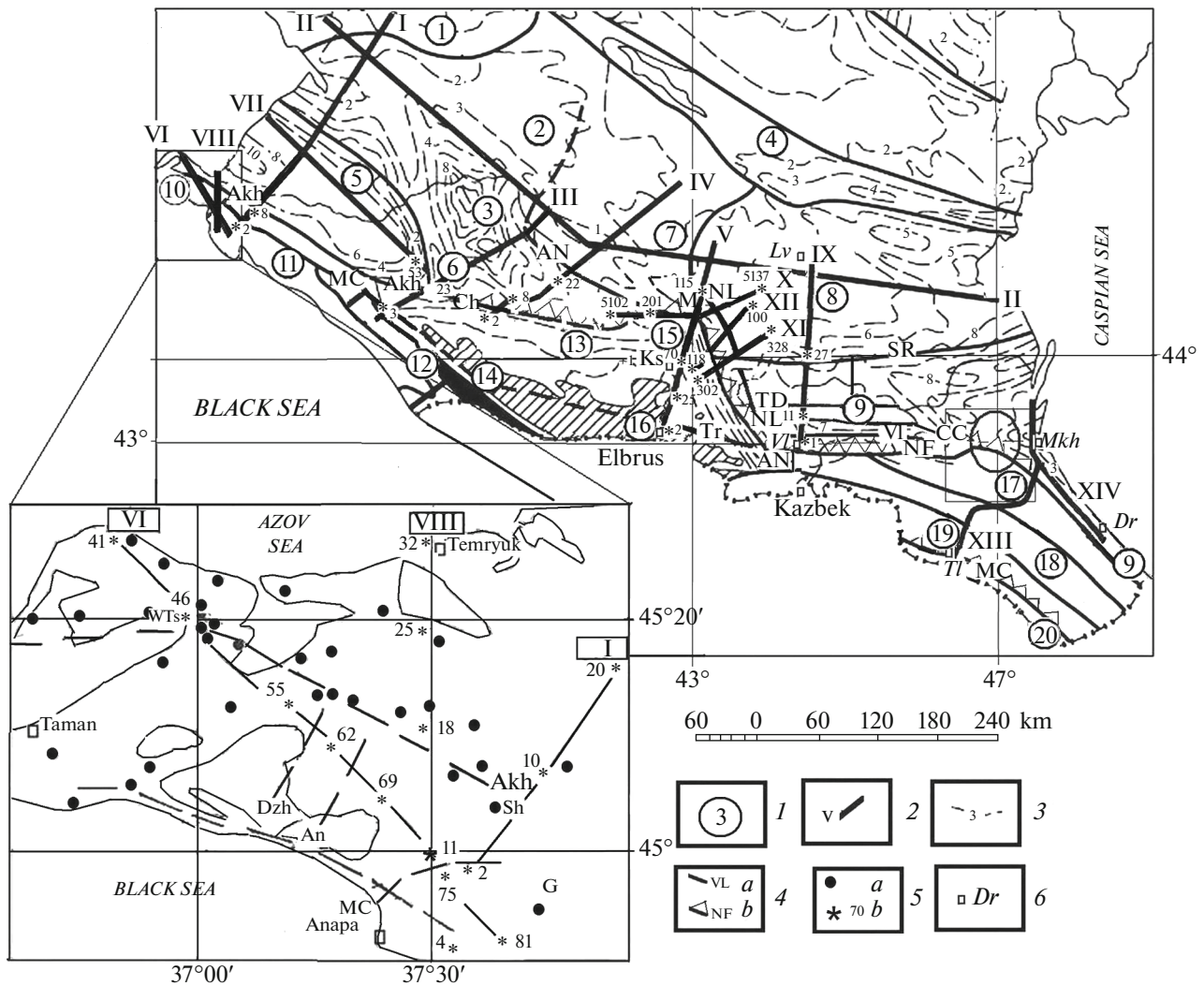


**Fig. 1.** Schematic location of MTS profiles on the schematic map of the North Caucasus structural zoning (*Atlas...*, 1998;<sup>1</sup> Neteba, et al., 1977). I—Structures: 1—Rostov outcrop; 2–9—Scythian Epi–Hercynian plate (2—Azov–Kuban depression; 3—East Kuban trough; 4—Manych trough zone; 5—Indolo–Kuban trough; 6—Aldygei outcrop; 7—Stavropol arch; 8—Terek–Kuma depression; 9—Terek–Caspian trough); 10–21—folded system of the Greater Caucasus (10—periclinal Taman trough; 11—Novorossiysk folded zone; 12—Paleozoic outcrops; 13—North Caucasus marginal massif; 14—Front Range zone; 15—Mineralnye Vody outcrop; 16, 20—Main Range of the Greater Caucasus; 17—Limestone Dagestan; 18—Agvali monocline; 19—Lateral Range); 2—ECWM, MTS profiles (*a*, *b*): I—Kuban, II—Yeisk–Caspian Sea, III—Tuapse, IV—Krasnaya Polyana, V—Near-Elbrus, VI—Taman–Novorossiysk, VII—Acheuev–Khodyzhensk, VIII—Novorossiysk–Temryuk, IX—Vladikavkaz–Levokumskoe, X, XI, XII—Mineralnye Vody outcrop, XIII—Talyarata–Makhachkala, XIV—Makhachkala–Derbent; 3—depth isolines of the Cimmerian pre–collision complexes (crystalline basement); 4, *a*—faults (AN—Anapa, AN—Armavir–Nevinnomyssk, Akh—Akhtyr, VL—Vladikavkaz, MC—Main Caucasian, Dzh—Dzhiginka, CC—Ciscaucasian, SR—Sredinnyi, Tr—Tyrnyauz, Ch—Cherkessk); *b*—overthrusts (NF—Northern frontal of the Eastern Caucasus, TD—Terek–Derbent, MGC—Main of the Greater Caucasus; M—Mineralnye Vody, NL—Naguta–Lysaya Gora (boundaries of the Nalchik–Mineralnye Vody flexural–rupture zone)); 5: *a*—mud volcanoes (Sobisevich et al., 2005); Sh—Shugo, G—Gladkovsky, WTs—Western Tsimbal; *b*—MTS o.p.; 6—cities: Ks—Kislovodsk, Lv—Levokumsk, VI—Vladikavkaz, Mkh—Makhachkala, Dr—Derbent, TI—Talyarata, ST—Stavropol. The circle is the region where the most hypocenters of crustal earthquakes (7–8 MSK) are concentrated. The square is the region of the Dagestan wedge.

meganticlinorium. They were formed under northeastern tangential regional compression in the Alpine and Late Alpine collisional stages of development. At this time, the Akhtyr fault with the northern dip of the mixer served as the main overthrust surface (Belov et al., 1990).

During the Late Alpine period, the Greater Caucasus nappe–folded structures were formed, under which the crustal thickness increases to 50–60 km from 43–45 km under the Stavropol arch and the Mineralnye Vody outcrop (Shempelev et al., 2020).

The pre-Hercynian basement sinks within the Indol–Kuban and Terek–Caspian troughs to depths of 10–14 km, and the folded basement (pre-Jurassic) sinks to a depth of 9 km (*Atlas...*, 1998). The North Caucasus marginal massif is characterized by longitudinal wave velocities  $V_p = 6.4$  km/s at a depth of 20 km and  $V_p = 6.2$  km/s under its surrounding troughs, which is associated with their increased granitization (Belyavsky et al., 2007).

The maximum density of MT observations is in the northeastern part of the North Caucasus massif, which is considered to be a zone of stable seismic activity at the level of moderate and weak earthquakes. It includes the Nalchik–Mineralnye Vody flexural–rupture zone, which joins the Cherkessk fault, which bounds the Mineralnye Vody outcrop from the north (Fig. 1). Two north–northwest trending parallel zones of higher seismicity extend along this zone with a developed system of steeply dipping faults (Gabsarova et al., 2020).

#### MAGNETOTELLURIC STUDIES OF THE CENTRAL SECTOR OF THE NORTHERN CAUCASUS

In the central part of the North Caucasus, magnetotelluric observations were considered on the following profiles: Krasnaya Polyana (**IV**), Near–Elbrus (**V**) and **X**, **XI**, **XII**, intersecting the North Caucasus marginal massif (Fig. 1). The distribution of electrical conductivity was evaluated under the Main Range of the Greater Caucasus, the North Caucasus marginal massif, the Mineralnye Vody outcrop, the Stavropol arch, and in the East Kuban and Terek–Caspian troughs. MT soundings were performed in the range of periods  $0.001 < T < 1000$  s by means of CES-2, CES-M and MTU-5, MTU-2 stations with a station interval of 1–5 km by OOO Electromagnetic Research Center, OOO Severo-Zapad, and Kavkazgeolsyemka Association.

The primary processing of magnetotelluric observations was carried out by OOO Electromagnetic Research Center, OOO Severo-Zapad, and the advanced processing by the GEON Center and the Geoelectromagnetic Research Center of the branch of the Institute of the Physics of the Earth. The results of the control observations made with the MTU stations showed that in synchronous measurements with the base station, the relative arithmetic mean deviations of the main scalar impedances are 1–1.6%, those of the additional ones are 4–4.5%, the phase errors of the main impedances are  $1.3^\circ$ , and those of the additional ones are  $4^\circ$ . The three-dimensional interpretation of the  $[Z_{ob}]$  matrix components was performed for the areas:  $4 \times 10^4$  km<sup>2</sup>, including MTS profiles **IV**, **V**, **X**, **XI**, **XII**, and  $10^4$  km<sup>2</sup>, excluding profile **IV**.

#### THREE-DIMENSIONAL INTERPRETATION OF MAGNETOTELLURIC DATA

The 3D interpretation of the magnetotelluric data was performed in the following steps:

- Evaluating the resolution ability of the 3D inversion software WSINV3DMT to reconstruct the electrical resistivity (ER) distribution  $\rho_m(X_m, Y_m, Z_m)$  from its inversion values  $\rho_{in}(X_{in}, Y_{in}, Z_{in})$  in the test 3D models corresponding to the previously constructed geoelectric 3D models of the region (Belyavsky, 2007).

- Making starting and test models based on: one-dimensional and two-dimensional inversions (Belyavsky, 2007; Varentsov, 2002) of the main components of the experimental impedance tensors  $[Z^{ob}]$  and their invariant values—maximum  $Z_{ob}^{max H}$  and minimum  $Z_{ob}^{min H}$  induction impedances (Council et al., 1986); interactive fitting of the 3D model  $\rho_m^{max H}$ ,  $\rho_m^{min H}$  to the curves  $\rho_{ob}^{max H}$  and  $\rho_{ob}^{min H}$ . The latter problem was solved with a block adapted to the Maxwell software, which performs various types of transformations of matrices  $[Z^{ob}]$  and their 1D inversion.

- Calculating the deviations of the impedance tensor components  $[Z^{in}]$  from the experimental ones  $[Z^{ob}]$  at the inversion points (i.p.), in order to see if the obtained inversion values  $\rho_{in}(X_{in}, Y_{in}, Z_{in})$  adequately correspond to the geoelectric parameters of the studied objects.

- Analyzing whether the distributions  $\rho_{in}(X_{in}, Y_{in}, Z_{in})$  correspond to seismic constructions and evaluating the content of the fluid water fraction in the low-resistance anomalies.

The three-dimensional inversion software WSINV3DMT is based on the Occam's principle: minimizing the Tikhonov residual functional with weight characteristics in the initial and model data, obtaining the smoothest characteristics of the geoelectric section. The minimization is performed by means of the approximate Gauss–Newton linearization method. As a result, distributions of the inversion values  $\rho_{in}(X_{in}, Y_{in}, Z_{in})$  smoothed along the MTS profiles are obtained. The  $X$ -axis is oriented north and the  $Y$ -axis is oriented east. The direct MT problem was solved by the finite-difference method (Siripunvaraporn et al., 2005). The total deviation of all the initial components of the impedance tensor  $[Z^{ob}]$  from the matrices  $[Z^{in}]$  obtained at each iteration of the inversion process is estimated by the normalized standard deviation, the RMS parameter, which controls the achievement of the main minimum of the residual functional. In its absence, the components of the matrices  $[Z_{in}]$  obtained for the RMS minima, at which the largest approximation of the main components of the tensors  $[Z_{ob}]$  to  $[Z_{in}]$  was achieved in the vicinity of

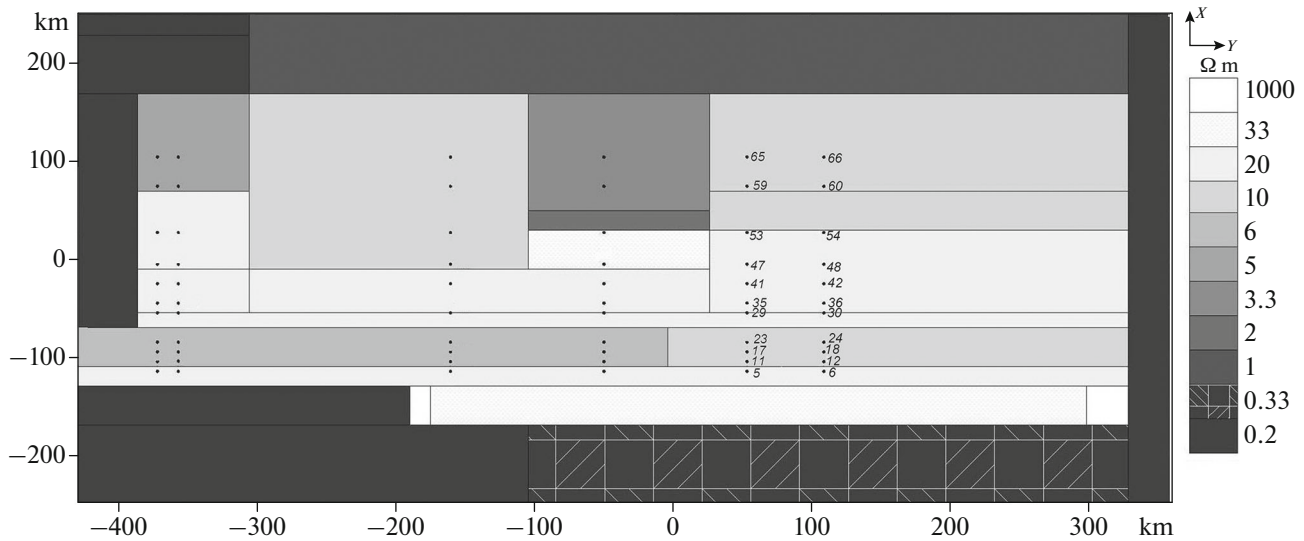


**Fig. 2.** Cross section at  $Z = 100$  m of the test 3D model of the North Caucasus. To the right is the resistivity scale of the upper model blocks ( $\rho_t$ ), ● are the inversion points [ $Z_t$ ]. Their numbers are shown in italics for Pr. 5 (i.p. 5–65), corresponding to the position of Pr. V in Fig. 1, and Pr. 6 (i.p. 6–66).

low-resistance anomalies, were considered. The inverse MT problem was solved in 15–25 iterations.

Due to the large amount of magnetotelluric data (more than 1000 MTS o.p. on profiles up to 2300 km long) and the limited ability of the WSINV3DMT software to invert all impedance tensors simultaneously, the 3D inversion was performed separately for the western, central and eastern parts of the North Caucasus. We identified structures within which it would be sufficient to perform 1D/2D inversions, thus reducing the number of 3D invertible tensors [ $Z_{ob}$ ]. In the central part of the North Caucasus, we considered MTS profiles IV, V, X, XI, and XII; in its western part, we inverted MT data on MTS Pr. VI, VII, VIII and partly on Pr. I, II, III (Belyavsky, 2023), and in the eastern part, on Pr. IX, XIII, and XIV (Belyavsky, 2022) (Fig. 1).

We solved the inverse problem for a series of starting models, from which we selected the one that provided the minimum relative arithmetic mean deviations ( $\delta_{xy}$ ,  $\delta_{yx}$ ) of the experimental ones  $|Z_{ob}^{xy}|$ ,  $|Z_{ob}^{yx}|$  from the model ones  $|Z_{in}^{xy}|$ ,  $|Z_{in}^{yx}|$  and impedance phases  $\text{Arg}Z_{ob}^{xy}$ ,  $\text{Arg}Z_{ob}^{yx}$  from  $\text{Arg}Z_{in}^{xy}$ ,  $\text{Arg}Z_{in}^{yx}$  in MTS o.p., under which the anomalies of increased conductivity are mapped.

*Studies Based on 3D Test Models of Three-Dimensional Inversion Sensitivity*

Three-dimensional inversion experiments (WSINV3DMT) were performed on test tensors [ $Z_t$ ] of the 3D model (Fig. 2) constructed by fitting the 3D

model  $\rho_t^{\max H}(T)$  and  $\rho_t^{\min H}(T)$  to the curves  $\rho_{ob}^{\max H}(T)$ ,  $\rho_{ob}^{\min H}(T)$  along profiles 5 (i.p. 5–65) and 6 (i.p. 6–66). The azimuths of the model profiles were  $30^\circ$  and are close to the orientation of the experimental MTS profiles (Fig. 1). The starting models in the three-dimensional inversion contained blocks with averaged values— $\rho_t$  in the upper layer, and low-resistance troughs flanking the high-resistance North Caucasian marginal massif in the lower layer. The upper layer was overlain by a 150 m thick plate with  $\rho_t = 10 \Omega \text{ m}$ , which reduced the errors in the calculation of the EM fields when blocks with a significant contrast in  $\rho_t$  were joined (Miensopust et al., 2013). A series of 3D inversions performed for the matrices [ $Z_t$ ] with different starting models showed that it is possible to use the WSINV3DMT software to estimate the parameters of the lower conducting blocks under profiles 5 and 6 (Figs. 3b, 4c).

The position of the top of the conducting blocks located under the inhomogeneous upper layer in i.p. 5–41 of profile 5 corresponds to the maximum gradient of the change in  $\rho_{in}(X_{in}, Y_{in}, Z_{in})$  in the low-resistance anomalies (Figs. 3a, 3b) obtained during 14 iterations of the inversion process (RMS = 4.3). The integral conductivity of the conducting test blocks  $S_t = 2000 \text{ S}$  in i.p. 35 is higher than  $S_{in} \approx 1000 \text{ S}$ ; however, under i.p. 41, where  $S_t = 1700 \text{ S}$ , it is close to  $S_{in} = 1500\text{--}1600 \text{ S}$  (Fig. 3b). The closeness of the distribution  $\rho_{in}(X_{in}, Y_{in}, Z_{in})$  to the model distribution  $\rho_t(X_t, Y_t, Z_t)$  in the period interval  $0.1 < T < 300 \text{ s}$  corresponds to the deviations  $\delta_{xy} = 1\text{--}25\%$  and  $\delta_{yx} = 1\text{--}12\%$  of the

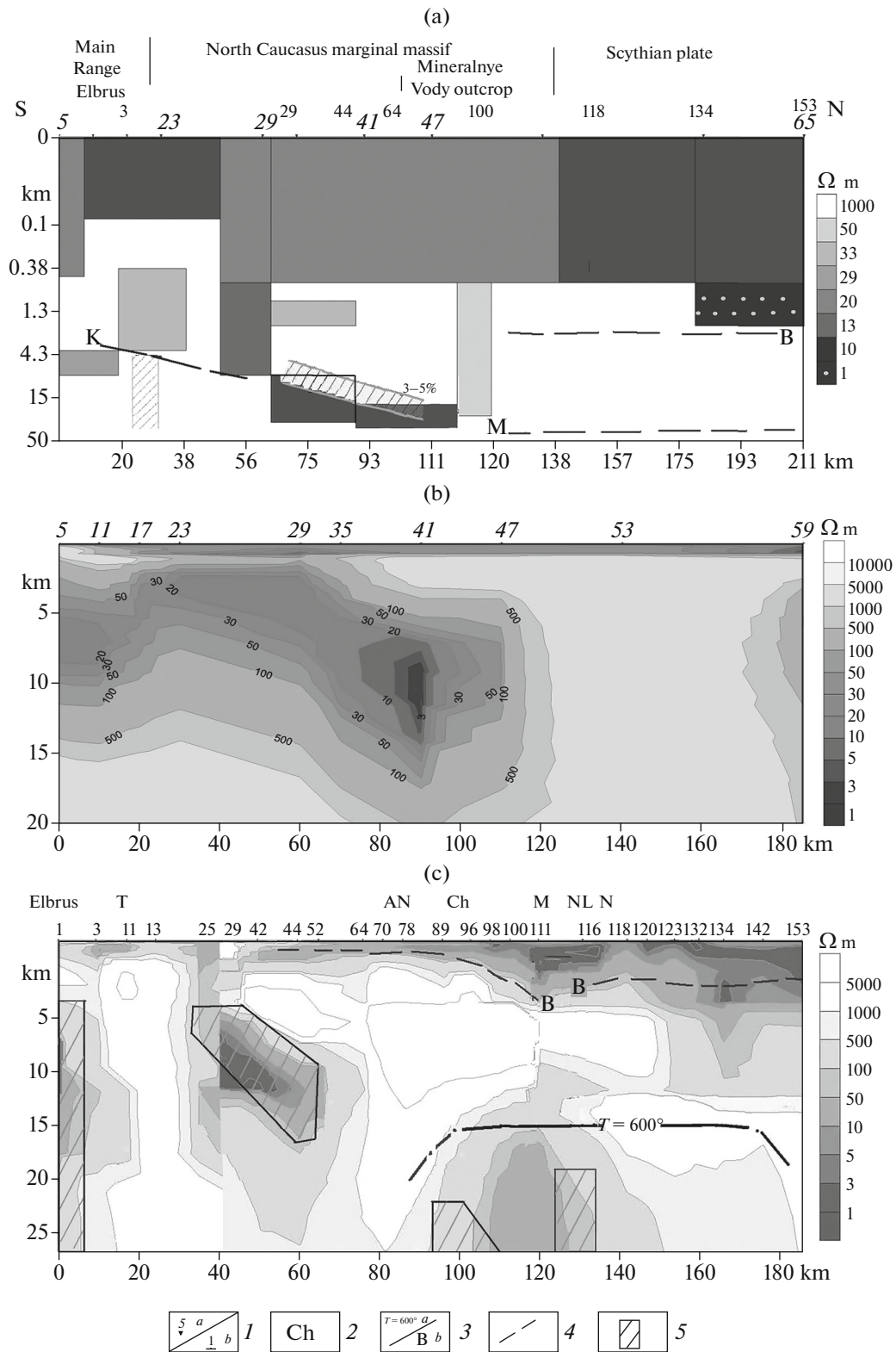


**Fig. 3.** The Near–Elbrus profile (Pr. V), three–dimensional interpretation results: (a)—by the method of fitting the parameters of 3D models (Fig. 2) (Belyavsky, 2007), the scale along the depth axis is logarithmic; (b), (c)—3D inversion (WSINW3DMT) of the test matrices  $[Z_t]$  of the model (b) and experimental  $[Z_{ob}]$  (c). Legend: 1—the position and numbers of:  $a$ —model i.p.,  $b$ —experimental o.p.; 2—abbreviations of faults according to Fig. 1; 3—position of the isotherm with  $T = 600^\circ\text{C}$  (a) and the top of the basement (b); 4—the Moho (M) and Conrad (K) boundaries (Atlas..., 1998); 5—blocks with 3–5% deficit in the velocity of longitudinal waves (Shempelev et al., 2020).



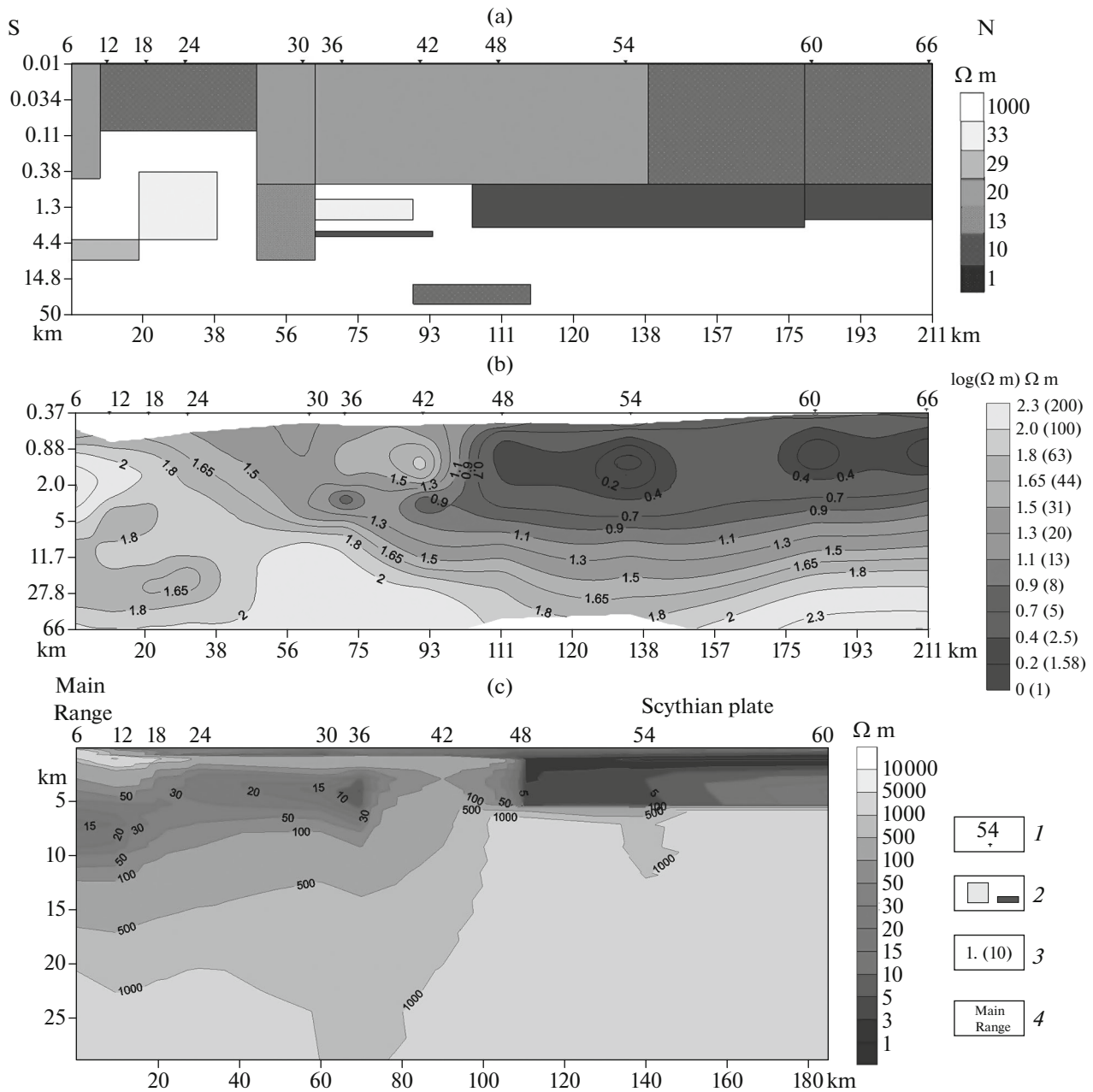


**Fig. 4.** Results of one-dimensional inversions of curves  $\rho'_{yx}$  (b) and three-dimensional matrices  $[Z_i]$  (c) in the test 3D model (a) for Pr. 6 (i.p. 6–66, Fig. 2). Legend: 1—i.p.; 2—model blocks; 3—resistivity scale in logarithmic and linear scales; 4—names of structures.

impedances  $|Z_t^{xy}|$  and  $|Z_t^{yx}|$  from those obtained with the 3D inversion  $|Z_{in}^{xy}|$  and  $|Z_{in}^{yx}|$ .

Figure 4 shows the results of the one-dimensional inversion of the curves  $\rho'_{yx}$  (Fig. 4b) and the three-dimensional inversion of the impedance matrix components  $[Z_i]$  (Fig. 4d) for Pr. 6. In the test model, there is no block with  $\rho_t = 10 \Omega \text{ m}$  under Pr. 6 at depths of 9–29 km (i.p. 30–42), which is present under Pr. 5

(Fig. 3a). The one-dimensional inversion of the curves  $\rho'_{yx} \approx \rho^l$  reflected the change in  $\rho_t$  of the upper structural level, the sedimentary cover, the fault under i.p. 30, and the conducting block under i.p. 36–42 (Fig. 4b). However, it did not reveal the conducting block under i.p. 6–12. The three-dimensional inversion showed the block, with corrected parameters of low-resistance anomalies under i.p. 18–42. The obtained  $S_{in}$  are close to the test  $S_t$  in i.p.: 6–12, where

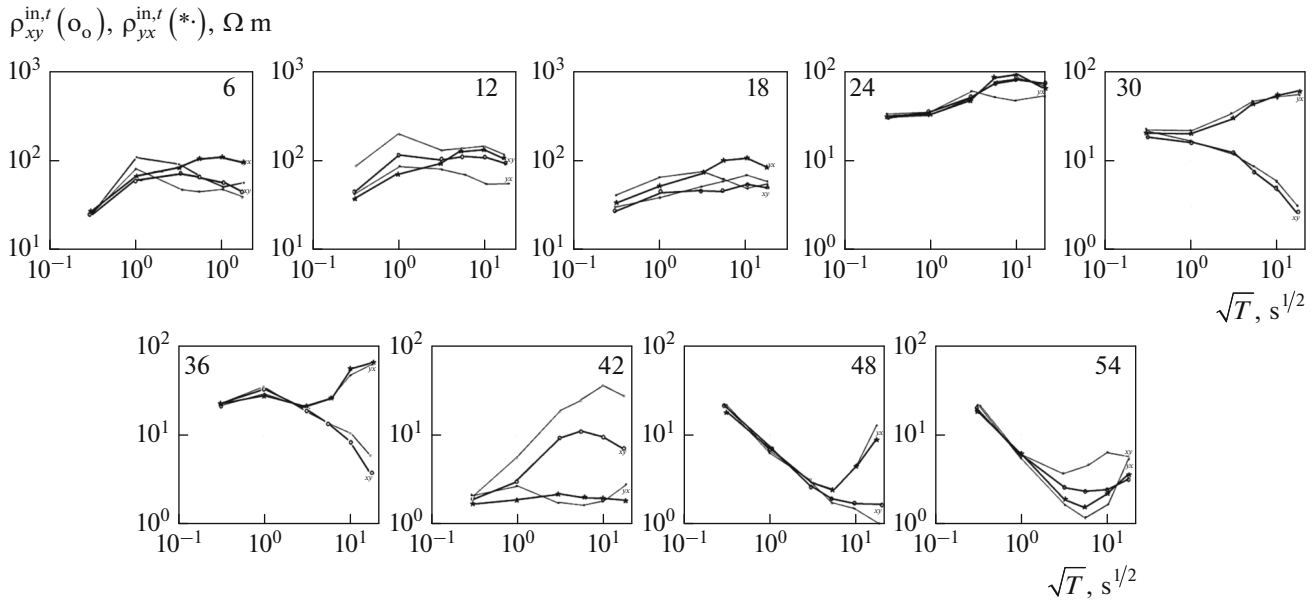


**Fig. 5.** Apparent resistivity curves ( $\rho_{yx}^{in,t}, \rho_{xy}^{in,t}$ ) for the cross section of the test 3D model (Fig. 4). The thick lines are the curves  $\rho_{yx}^{in}$  and  $\rho_{xy}^{in}$ , and the thin lines are the corresponding 3D inversions of the test  $\rho_{yx}^t, \rho_{xy}^t$ .

$S_t = 170$  S and  $S_{in} = 200–250$  S; 18–24, where  $S_t = 120$  S and  $S_{in} \approx 150–200$  S; 30, where  $S_t = 500$  S and  $S_{in} \approx 170–200$  S; 36, where  $S_t = 600$  S and  $S_{in} \approx 350–500$  S.

Figure 5 shows the test curves  $\rho_{xy}^t(T), \rho_{yx}^t(T)$  and the inversion curves  $\rho_{xy}^{in}(T), \rho_{yx}^{in}(T)$ . For i.p. 6–18, the deviation values are  $\delta_{yx} = 5–35\%$  and  $\delta_{xy} = 1–25\%$ , in i.p. 24– $\delta_{yx} = 1–25\%$  and  $\delta_{xy} = 0.5–5\%$ , 30  $\delta_{yx} = 1–10\%$ ,  $\delta_{xy} = 0.5–10\%$ . The minimum  $\delta_{yx}$  are in i.p. 30–54.

For other sections of the test model, the 3D inversion experiments (Belyavsky, 2023) also showed that the WSINV3DMT software (given the effect of the equivalence principle and the appearance of conductivity pseudo-anomalies) restores the parameters of the low-resistance blocks located under the inhomogeneous top layer. The deviation of the obtained  $\rho_{in}$  from the test  $\rho_t$  can reach 100–200%, but the integral conductivity  $S_{in}(X_{in}, Y_{in}, Z_{in})$  is close to the test  $S_t$ , and so is the maximum gradient of the decrease in  $\rho_{in}(X_{in}, Y_{in}, Z_{in})$  along the  $Z$ -axis to the position of the top of the low-resistance blocks.

*Starting Geoelectric Models of the Central Part of the North Caucasus*

On the experimental MTS profiles, where 1D/2D inversions of the invariant components of the impedance tensors  $[Z_{ob}]$  are sufficient, the geoelectric sections previously obtained for the Stavropol arch, the Indol–Kuban and the East Kuban troughs (Belyavsky

et al., 2007) were included in the starting 3D models. With the three-dimensional dimensionality of the medium determined by the asymmetry parameters of the matrices  $[Z_{ob}]$  (Berdichevsky and Dmitriev, 2009)  $skew = |Z_{xx} + Z_{yy}|/|Z_{xy} - Z_{yx}|$  and  $skew\eta = [Im(Z_{xy}Z_{yy}^* + Z_{xx}Z_{yx}^*)]^{1/2}/|Z_{xy} - Z_{yx}|$ , we constructed models incorporating the results obtained by fitting the 3D model curves  $\rho_m^{max H}(T)$  and  $\rho_m^{min H}(T)$  to the experimental curves  $\rho_{ob}^{max H}(T)$  and  $\rho_{ob}^{min H}(T)$ .

To achieve maximum agreement between the components  $[Z_{ob}]$  and  $[Z_{in}]$ , we varied the parameters of the model blocks, the size of their sampling grids and the number of inverted impedance tensors in the starting models. We considered about 30 starting models for the central part of the North Caucasus, with different numbers of sampling cells. We set the following number of such cells: in type 1 models—46 on the  $X$ -axis; 50 on the  $Y$ -axis; 20 on the  $Z$ -axis, with a 5 km interval between grid nodes (on the  $X$ -axis and  $Y$ -axis); in type 2 models—34 grid cells on the  $X$ -axis, 50 on the  $Y$ -axis, and 20 on the  $Z$ -axis, with a 3 km interval. In the starting models, we inserted blocks into the upper layer,  $\Delta H = 150$  m thick, with  $\rho_m = 10$   $\Omega$  m, which had the following  $\rho_m$ : 100  $\Omega$  m, 1000  $\Omega$  m (outcrops of the folded basement), and 5–20  $\Omega$  m (depressions and troughs). The blocks below approximated the change in conductivity of troughs and uplifts (1D/2D inversion and 3D modeling data).



*Near-Elbrus profile (Pr. V)*

Within the Main Caucasian Range, skew and skew  $\eta$  asymmetry parameters are  $>0.3$  at medium and low frequencies, indicating a three-dimensional distribution of the ER (Belyavsky, 2007). The curves  $\rho_{ob}^{maxH}$  at medium frequencies are oriented along the following azimuths:  $(-10^\circ)-(-40^\circ)$  on the Main Range of the Greater Caucasus,  $-10^\circ-50^\circ$  within the North Caucasus monocline, and  $-30^\circ$  to  $70^\circ$  in the Terek-Kuma depression (Fig. 1). By fitting the 3D model curves  $\rho_m^{maxH}$ ,  $\rho_m^{minH}$  to  $\rho_{ob}^{maxH}$  and  $\rho_{ob}^{minH}$ , we found blocks under: the Main Caucasian Range (o.p. 1–3) with  $\rho_m \approx 30 \Omega \text{ m}$  and the North Caucasus marginal massif (o.p. 29–100) with  $\rho_m \approx 10-15 \Omega \text{ m}$  (Fig. 3a).

*Krasnaya Polyana profile (Pr. IV)*

According to the distribution of the asymmetry parameters, at frequencies below 1 Hz, areas of quasi-dimensional dimensionality—skew  $< 0.15$ —are located under the Stavropol arch and in the East Kuban trough. At low frequencies, the impedances  $Z_{ob}^{maxH}$  are oriented along azimuths of  $70^\circ-90^\circ$ , while at medium frequencies, they are oriented along azimuths of  $-30^\circ-(-40^\circ)$  which are close to the structural lines of the region. The two-dimensional inversion of the curves  $\rho_{ob}^{maxH}$  and their phases  $\text{Arg}Z_{ob}^{maxH}$ , performed in the E-polarization mode (Fig. 6a), helped to find a block with  $\rho_{in} = 5 \Omega \text{ m}$  and thickness  $H_{in} = 20-30 \text{ km}$  under the Caucasus folded system (o.p. 2–3) at depths of  $Z_{in} = 10-12 \text{ km}$ . The 3D model fitting method split it in two, moving the upper block with  $\rho_{in} = 20 \Omega \text{ m}$  to a depth of 15 km, and the lower block with  $\rho_{in} = 40 \Omega \text{ m}$  to  $Z_{in} = 30 \text{ km}$ .

*Mineralnye Vody Outcrop Profiles (X, XI, XII)*

On profile X, skew  $< 0.2$  at high frequencies and skew  $> 0.2$  at low frequencies, so are the phase asymmetry parameters—skew $\eta$ . The curves  $\rho_m^{maxH}$ ,  $\rho_m^{minH}$  are oriented along azimuths of  $20^\circ-30^\circ$ . On profile XII, skew  $> 0.2$  at most o.p. In periods  $T > 40 \text{ s}$ , the curves  $\rho_m^{maxH}$  are oriented mainly along azimuths of  $100^\circ-120^\circ$  (Belyavsky, 2007). A similar situation can be observed on profile XI.

*Reliability of the Geoelectric Sections  
Obtained by 3D Inversion*

The correspondence between the experimental curves  $\rho_{ob}^{xy}$ ,  $\rho_{ob}^{yx}$  obtained with the 3D inversion and  $\rho_{in}^{xy}$ ,  $\rho_{in}^{yx}$  is a criterion for the reliability of the considered geoelectric sections. Their frequency characteristics

are shown in Fig. 7. It can be seen that for periods  $T > 10-50 \text{ s}$ , the WSINV3DMT software gives smoothed changes in the values of  $\rho_{in}^{xy}$ ,  $\rho_{in}^{yx}$  caused, on the curves  $\rho_{ob}^{xy}$  and  $\rho_{ob}^{yx}$ , by local inhomogeneities located under profiles X (a), XI (b), XII (c), V (d), and IV (e). This means that it partially dampens the “S effect” manifested on the curves  $\rho_{ob}^{xy}$ ,  $\rho_{ob}^{yx}$  when regional conductivity anomalies located in the lower part of the section are detected. Similar conclusions were reached for other MTS profiles (Belyavsky, 2022; 2023).

During the solution of the inverse MT problem, at 13–24 iterations of the inversion process, the RMS parameter decreased to RMS = 4.1–4.6. The model which was taken as the final version was the 3D model in which the minimum RMS values corresponded to the minimum deviations ( $\delta_{xy}$ ,  $\delta_{yx}$ ) of the experimental scalar impedances  $|Z_{ob}^{xy,yx}|$  from  $|Z_{in}^{xy,yx}|$  at the MTS i.p. under which the conductivity anomalies were found.

The distribution of  $\delta_{xy}$ ,  $\delta_{yx}$  for the central part of the North Caucasus is shown in Fig. 8, with their averaged values in the following periods being:

—  $T = 0.1-1 \text{ s}$ , Pr. X— $\delta_{yx,xy} = 1-5\%$  (rarely  $\delta_{yx,xy} = 10-15\%$ ), and on Pr. XII, XI— $\delta_{yx,xy} = 1-10\%$  (rarely  $\delta_{yx,xy} = 15-20\%$ );

—  $T = 10-300 \text{ s}$ , Pr. X and XII— $\delta_{xy} = 1-25\%$ ,  $\delta_{yx} = 1-12\%$  (rarely  $\delta_{xy,yx} > 20\%$ ) and on Pr. XI— $\delta_{yx} = 1-10\%$ ,  $\delta_{xy} = 1-35\%$ ;

—  $T = 0.1-300 \text{ s}$ , Pr. V— $\delta_{xy,yx} = 1-25\%$  (rarely  $\delta_{xy,yx} > 25\%$ ),

—  $T < 10 \text{ s}$ , Pr. IV— $\delta_{xy,yx} = 1-7\%$ , and for  $T = 10-400 \text{ s}$ — $\delta_{yx} = 5-20\%$  and  $\delta_{xy} = 10-60\%$ .

Above the low-resistance anomalies, in Fig. 8, they are shown by symbol V for the impedances  $Z_{ob}^{yx}$  oriented along the main structural lines ( $Z_{ob}^{\parallel}$ ) at the i.p. of the profiles:

— Pr. X, 5108— $\delta_{yx} < 25\%$ , 207  $\delta_{yx} < 10\%$ , 214–215, 220–221  $\delta_{yx} < 15\%$ .

— Pr. XII, 109 and 117— $\delta_{yx} < 15\%$ , 113 and 118— $\delta_{yx} < 30\%$ .

— Pr. XI, 303–314, 317— $\delta_{yx} < 15\%$ .

— Pr. V, 25— $\delta_{yx} < 50\%$ , i.p. 29— $\delta_{yx} < 25\%$  and i.p. 44— $\delta_{yx} < 15\%$ .

— Pr. IV, 2, 8 and 19— $\delta_{yx} < 20\%$ .

The higher values of errors in  $\delta_{xy}$  as compared to  $\delta_{yx}$  on Pr. IV are associated with the edge effect manifested on the impedances  $Z_{ob}^{xy}$  ( $Z_{ob}^{\perp}$ ) from the southern side of the Indol-Kuban trough. It is not fully offset by the reduction of the model  $|Z_{in}^{xy}|$  to the minimum values of the experimental  $|Z_{ob}^{xy}|$ . A similar situation

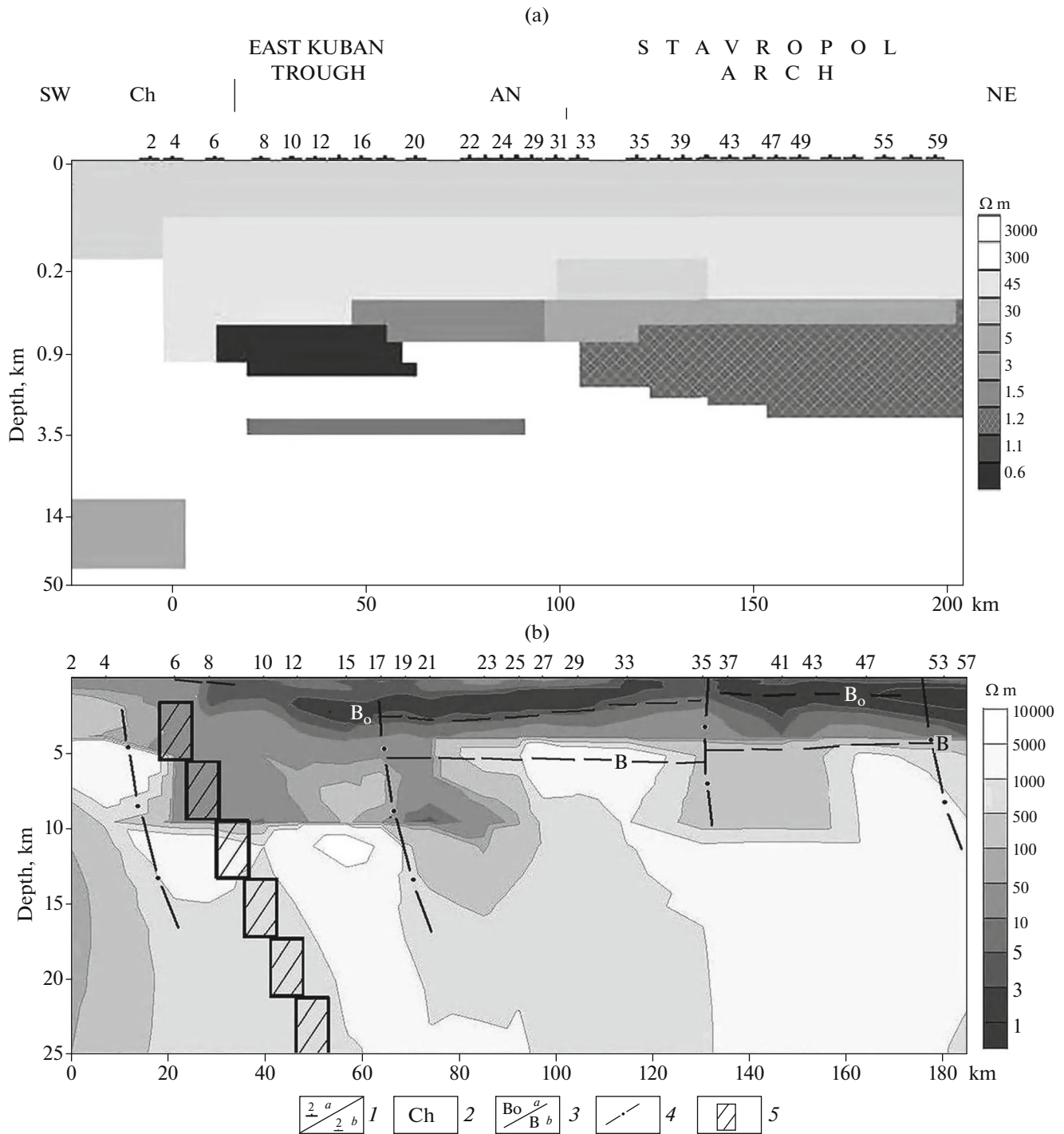


**Fig. 6.** Krasnaya Polyana profile (Pr. IV), the results of inversions of the experimental MTS curves: (a)—two-dimensional inversion of amplitude and phase E-polarization curves (depth scale is logarithmic); (b)—three-dimensional inversion of all components of the matrices  $[Z_{ob}]$ . Legend: 1—position of i.p. in 2D (a) and 3D (b) inversions; 2—abbreviations of deep faults (Fig. 1); 3—top of the folded basement (a) and the crystalline basement (ECWM) (b); 4—deep faults (ECWM); 5—zones of increased absorption of converted waves (Belyavsky et al., 2007).

can be observed on Pr. X, which extends along the northern boundary of the Mineralnye Vody outcrop, and on Pr. V, where the impedances  $Z_{ob}^{xy}$  are oriented close to the strike of the structural lines, and the errors

in  $\delta_{yx}$  are smaller than in  $\delta_{xy}$ . Low-impedance blocks in the lower part of the section appear mainly on longitudinal impedances  $Z_{in}^{\parallel}$ , but not on transverse ones— $Z_{in}^{\perp}$  which allows us to conclude that 3D inver-

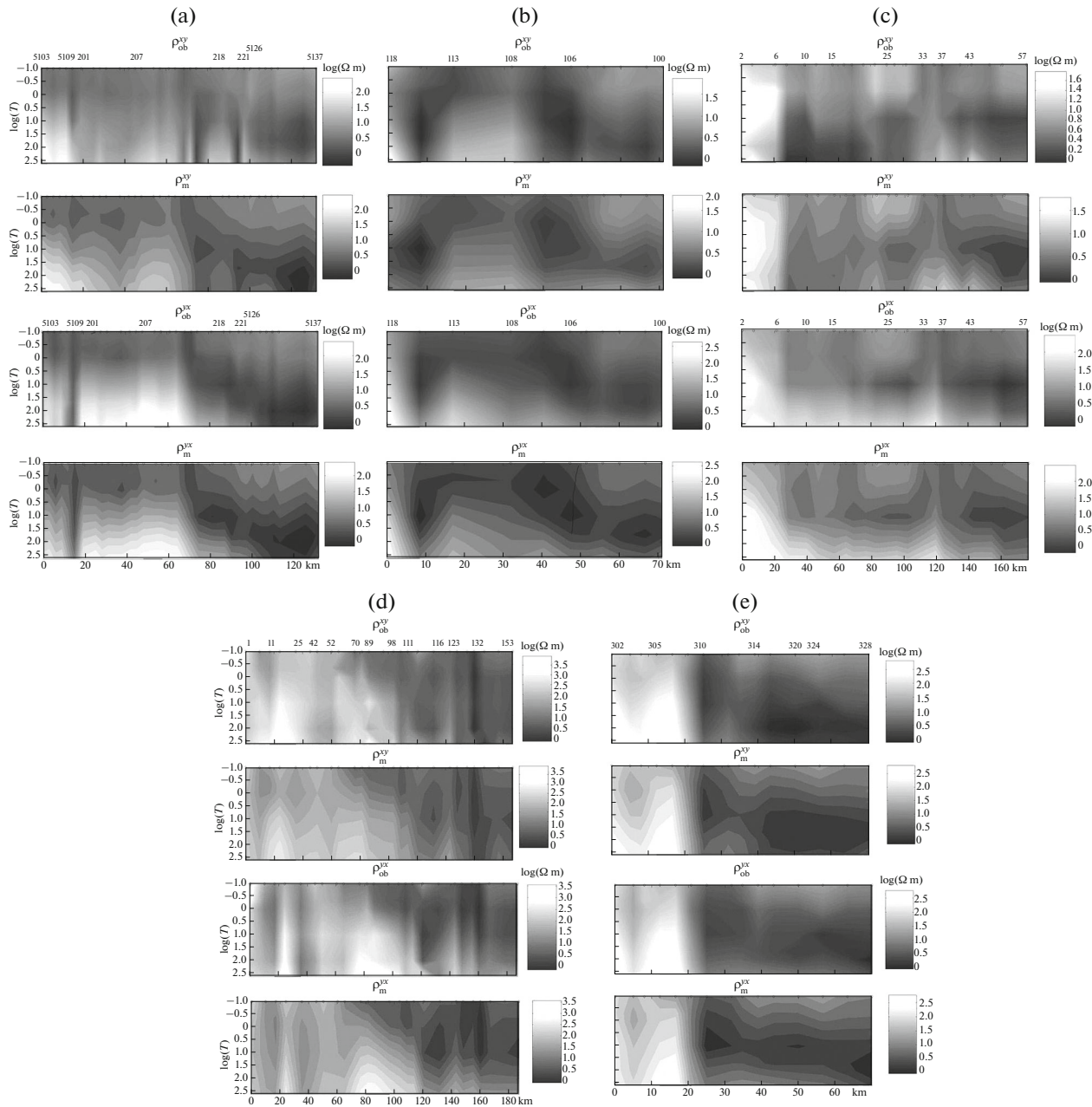


**Fig. 7.** Experimental ( $\rho_{ob}^{xy}$ ,  $\rho_{ob}^{yx}$ ) and inversion ( $\rho_{in}^{xy}$ ,  $\rho_{in}^{yx}$ ) maps of the apparent resistivity on the MTS profiles: **X** (a), **XI** (b), **IV** (c), **V** (d), and **XII** (e). Above is MTS i.p. To the right are resistivity scales in lg ( $\Omega$  m), to the left are periods in log ( $T$ , s).

sion can restore parameters of the geoelectric section and is confirmed by studies carried out on test models (Figs. 3, 4).

Within the Taman preclinal trough and the Novorossiysk folded zone (Belyavsky, 2023), the errors in  $\delta_{xy}$  and  $\delta_{yx}$  above the low-resistance blocks are:

– Pr. **VI**, near the Gladkovsky volcano  $\delta_{xy} \approx 50$ –70%,  $\delta_{yx} < 10\%$  (i.p. 80); for the Main Caucasian fault  $\delta_{xy} < 10\%$ ,  $\delta_{yx} = 20$ –60% (i.p. 74) and  $\delta_{xy} < 45\%$ ,  $\delta_{yx} =$

10–30% (i.p. 75); at the intersection of the Anapa and Moldavian faults  $\delta_{xy} \approx \delta_{yx} < 10\%$  (i.p. 63) and  $\delta_{xy} < 50\%$ ,  $\delta_{yx} < 20\%$  (i.p. 66), and at the intersection of of the Akhtyr and Dzhiginka faults  $\delta_{xy} \approx \delta_{yx} < 20\%$  (i.p. 59, 63).

– Pr. **VIII**, for the Main Caucasian fault  $\delta_{xy} \approx \delta_{yx} = 1$ –60% (i.p. 9–10); in the area of the Akhtyr fault  $\delta_{xy} \approx \delta_{yx} = 1$ –50% (i.p. 15),  $\delta_{xy} = 100$ –50%,  $\delta_{yx} = 10$ –50% (i.p. 16). On profiles **VI** and **VIII**, the MTS curves oriented along the faults (Fig. 1) have a smaller error in

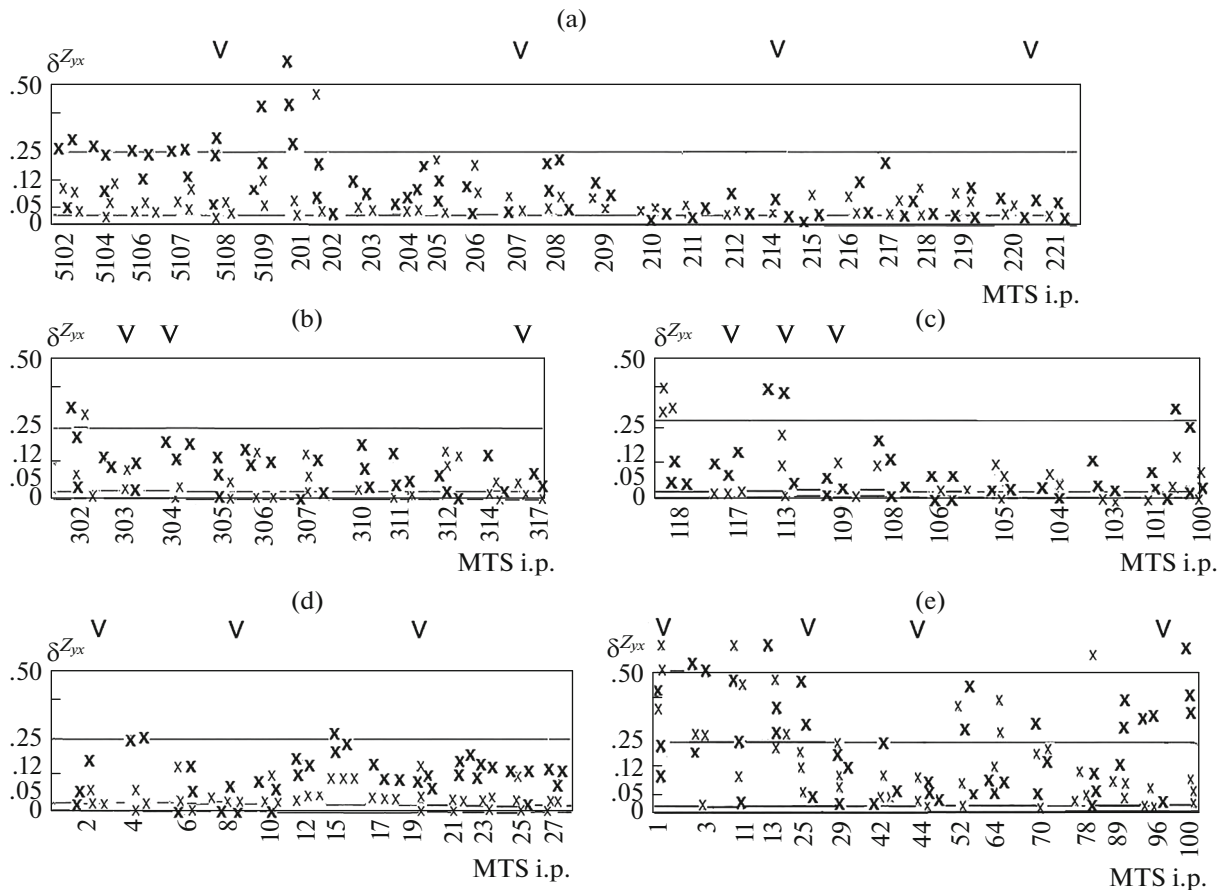


**Fig. 8.** Relative arithmetic mean errors ( $\delta_{zyx}$ ) of 3D inversion of the curves  $\rho_{ob}^{yx}$  on the MTS profiles: **X** (a), **XI** (b), **XII** (c), **IV** (d), and **V** (e). Small crosses—for the periods  $0.1 < T < 1$  s; large crosses—for the periods  $10 < T < 300$  s; **V**—low-resistance zones.

the deviation of the model curves from the experimental ones.

Within the eastern part of the North Caucasus, on Pr. **IX**, the curves oriented along the structural lines have the following  $\delta_{yx}$ : 1–20% (i.p. 1–3; 19), 1–10% (i.p. 11, 27, 52 and 68), and on Pr. **XIII**,  $\delta_{xy} \approx \delta_{yx} = 1$ –20% (i.p. 101–106),  $\delta_{xy} \approx \delta_{yx} = 1$ –50% (i.p. 107–114).

## GEOELECTRIC MODEL OF THE CENTRAL PART OF THE REGION

### *Krasnaya Polyana Profile*

The three-dimensional inversion of the matrices  $[Z_{ob}]$  corrected the parameters of the conducting block found by the 2D inversion under the northern side of the Greater Caucasus folded system (o.p. 2), making the values  $\rho_{in} = 50 \Omega \text{ m}$  in the depth interval of 10–25 km (Fig. 6b). Under this conductivity anomaly, deeper than 30 km, there is a domain (Belyavsky et al., 2007) with increased absorption of earthquake converted waves (ECWM), which flanks the Cherkessk fault. In the zone of transition from the East Kuban

trough to the North Caucasus monocline (o.p. 6–8), the anomaly with  $\rho_{in} = 10$ –50  $\Omega \text{ m}$  also correlates with the region of increased attenuation of converted waves, which sinks under the East Kuban trough. The region of increased conductivity at depths greater than 5 km under MTS 17–21 is close to the deep fault found by the ECWM method.

### *Near-Elbrus Profile*

Anomalies with  $\rho_{in} = 5$ –10  $\Omega \text{ m}$  are found under the Main Caucasian Range near the Elbrus volcano (o.p. 1–3) at depths of 5–20 km and within the Tyrnauz fault (o.p. 10–11) in the upper part of the section ( $Z_{in} < 1.5$  km) (Fig. 3c). Under the North Caucasian monocline from o.p. 25 to o.p. 64 (the Armavir–Nevnomysk fault), a block with  $\rho_{in} = 1$ –10  $\Omega \text{ m}$ , corresponding to the position of low-resistance blocks found by the fitting method, sinks from a depth of 5 to 15 km (Fig. 3a). Testing of the WSIN3DMT software showed (Fig. 3b) that they are found along their

entire length, so the distribution  $\rho_{in}(X_{in}, Y_{in}, Z_{in})$  given in Fig. 3c was applied.

These low-resistivity anomalies correlate with blocks of increased attenuation of earthquake converted waves (3– to 4-fold increase in absorption) and up to 3–5% deficit in longitudinal wave velocity (Fig. 3). This situation corresponds to the overthrust of the low-resistance, low-velocity block of the Scythian Plate, which led to the “throw-in of its layers” and the increase in crustal thickness under the Greater Caucasus orogeny (Shempelev et al., 2020).

The anomaly with  $\rho_{in} = 10\text{--}50 \Omega \text{ m}$ , located deeper than 15 km under o.p. 98–116, is associated with the system of faults bounding the Mineralnye Vody outcrop and the Stavropol arch (Fig. 3). It is found under the isotherm— $T = 600^\circ\text{C}$  (Levin and Kondorskaya, 1998), which indicates its possible connection with fluid saturation.

#### *Mineralnye Vody Outcrop Profiles*

The system of faults (Chegem, Mineralnye Vody and Naguta–Lysaya Gora faults) flanking the north–northwest trending Nalchik–Mineralnye Vody flexural–rupture zone (Figs. 9, 10) is characterized by anomalies  $\rho_{in} = 10\text{--}50 \Omega \text{ m}$  (o.p. 113–117) and  $\rho_{in} = 1\text{--}3 \Omega \text{ m}$  (o.p. 312–314, o.p. 108–109) at depths of 5–20 km. The anomalies found under Pr. X–XI (Figs. 7a, 7b) at depths of:  $Z_{in} = 10 \text{ km}$  with  $\rho_{in} = 3\text{--}10 \Omega \text{ m}$  (o.p. 5109, o.p. 207–208);  $Z_{in} = 20 \text{ km}$  with  $\rho_{in} = 50\text{--}100 \Omega \text{ m}$  (o.p. 214–216, o.p. 303–304; o.p. 117) and with  $\rho_{in} = 2\text{--}5 \Omega \text{ m}$  in o.p. 108–109, correlate with the position of the Armavir–Nevinnomyssk, Mineralnye Vody, and Naguta–Lysaya Gora faults.

Under the Mineralnye Vody outcrop, the anomalies of increased conductivity (Pr. V, X, XII) are consistent with the boundaries of the Elbrus–Mineralnye Vody shear fault zone (Milanovskii et al., 1989) and with the deep faults bounding the Nalchik–Mineralnye Vody flexural–rupture zone. Earthquake epicenters are concentrated along it (Gabsatarova et al., 2020), adjoining or including parts of the local zones of the decrease in longitudinal wave velocity and electrical resistivity under the Mineralnye Vody outcrop and the North Caucasus marginal massif (Figs. 9, 10a, 10c). East of the North Caucasus marginal massif (Figs. 9a, 9c; o.p. 218–5132, 118–108), the decrease in the velocity of longitudinal waves is explained by the increase in  $\text{SiO}_2$  content (from 63 to 65%), given the change in the velocity of transverse waves (Bulin and Egorkin, 2000).

#### SOURCE OF INCREASED CRUSTAL CONDUCTIVITY

The origin of the free fluid fraction and fluid transport pathways can be related to: magmatic form of its transfer from the mantle, transformation of serpentinites, dehydration of rocks, phase transformations of minerals, dilatancy processes, and fluid accumulation in the zones of transition from a more brittle to a more rigid crust.

The high permeability of the suture zones bounding the North Caucasus marginal massif is also evidenced by the fact that their helium concentration is 4 orders of magnitude higher than the reference value (Sobisevich et al., 2005). The main argument for fluid-saturated conducting crustal blocks is their correlation with domains of increased absorption and seismic wave velocity deficit. It is unlikely that graphitized formations are a source of low resistivity with a velocity deficit of up to 3–5% in the same conducting blocks. When the longitudinal wave velocity in graphite  $V_p = 4.3 \text{ km/s}$ , the graphite content in low-velocity blocks should reach 6–10% (Belyavsky, 2007), and no such evidence was found.

The decrease in resistivity at depths where the temperature reaches  $600^\circ\text{C}$  can be explained by the release of water from water-bearing minerals (Brown and Mussett, 1984), such as dehydration of serpentinites at  $T = 500^\circ\text{C}$  or amphibolite facies metamorphic rocks at  $T = 680^\circ\text{C}$ . Such temperatures cause thermal decomposition and a decrease in resistivity by two orders of magnitude (Zonov et al., 1989). The temperature reaches the required level of  $600^\circ\text{C}$  at depths of 15–20 km under the Stavropol arch and the Mineralnye Vody outcrop (Figs. 3, 9). The increased heat flux observed here is associated with crustal asthenolenses (Levin and Kondorskaya, 1998). GPS surveys showed that the structures of the Greater Caucasus are currently expanding. The overthrusts that are common here are caused by subhorizontal compressional stresses and “the introduction of mineral matter by upward flow of deep fluids...” (Lukk and Shevchenko, 2019). The fact that the intracrustal hydrogeothermosphere is possible at depths of 8–15 km, where more than 90% of earthquakes are concentrated, is also substantiated in the paper by (Kurbanov, 2001).

#### ESTIMATION OF FLUID CONTENT IN THE NORTH CAUCASUS REGION

The content of the fluid water fractions  $f_p$  bound in conductive circuits was determined according to the dependence of the electrical resistivity  $\rho$  in two-phase rocks on  $\rho_s$  of its skeleton and  $\rho_f$  of the fluid filling the pores (Shankland and Waff, 1977). At  $f_p < 15\%$ , the total binding of the fluid in the circuits conducting the current,  $\rho_f \ll \rho$ . The fluid content is then estimated by



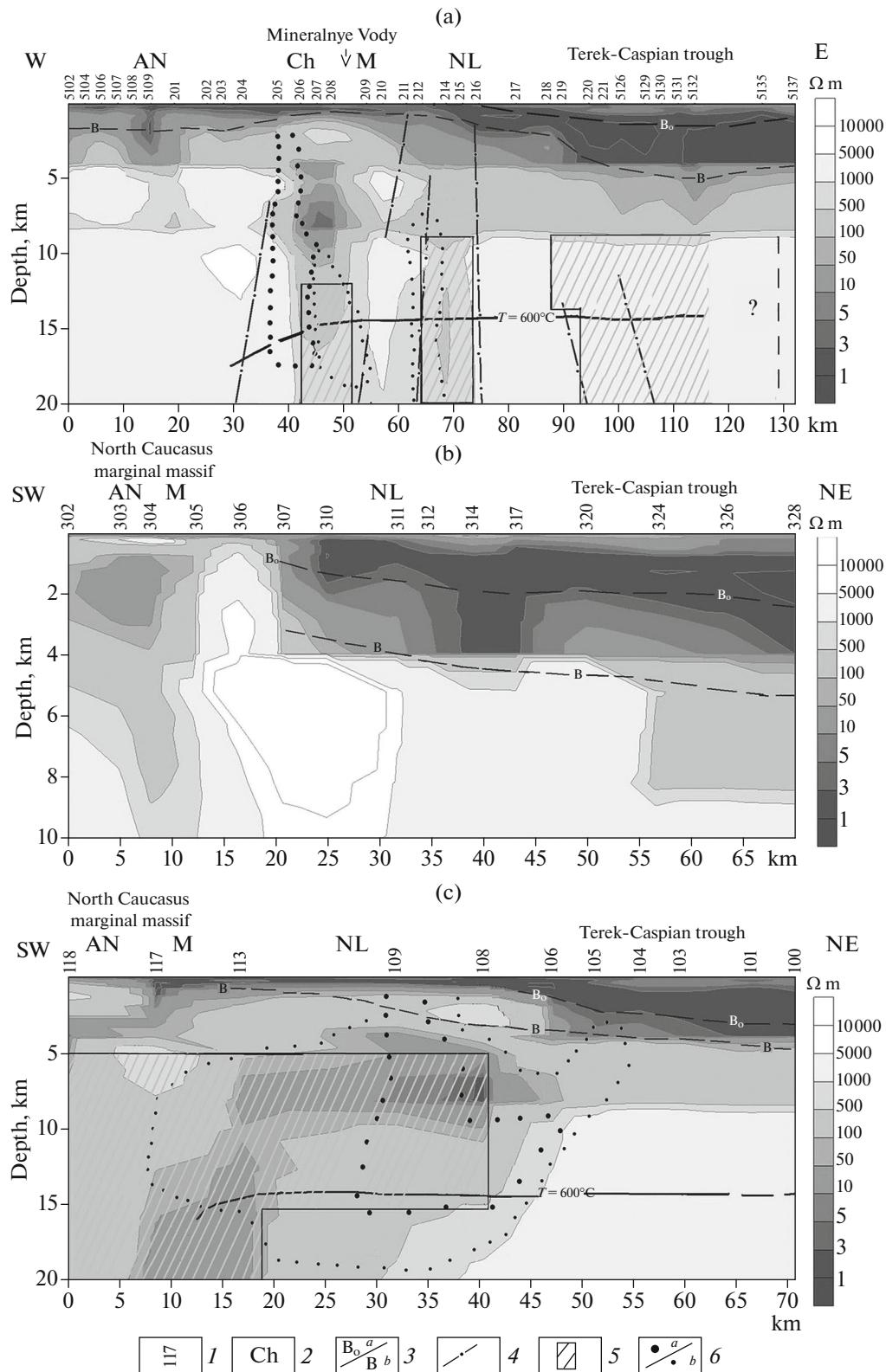


**Fig. 9.** Geoelectric sections (WSINW3DMT software) along the MTS profiles (Fig. 1): (a)—X, (b)—XII, (c)—XI. Legend: 1—MTS i.p.; 2—deep faults (Fig. 1); 3—top of the folded basement (a) and the crystalline basement (b) (*Atlas...*, 1998); 4—faults found from seismic data; 5—blocks with decreased  $\Delta V_p = 2-4\%$  relative to average velocities; 6—boundaries of high (a) and less high (b) earthquake concentration regions.



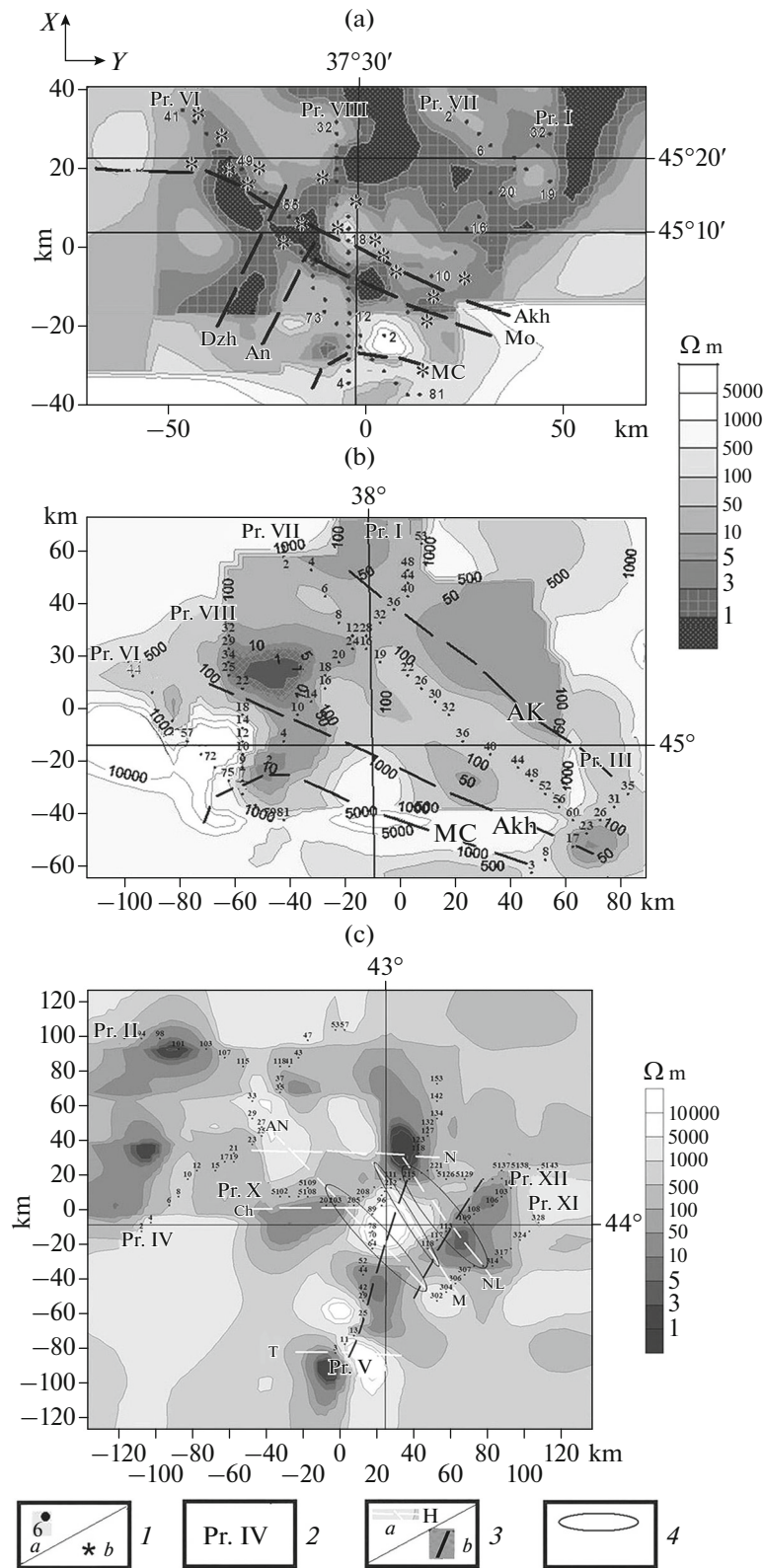


**Fig. 10.** Resistivity distribution (3D inversion) at depths of: (a)—5.5 km; (b)—8.6 km (western part of the North Caucasus); (c)—6.6 km (central part of the North Caucasus); 1 (*a*—MTS numbers (every second o.p.); *b*—mud volcanoes); 2—MTS profiles; 3 (*a*—deep and regional faults (Fig. 1), *b*—boundaries of the Elbrus–Mineralnye Vody zone of wrench faults (Milanovskii et al, 1989), the Mineralnye Vody (M) and Naguta–Lysaya Gora (NL) deep faults (Fig. 1) bounding the Nalchik–Mineralnye Vody flexural–rupture zone); 4—earthquake epicenter concentration regions (Gabsatarova et al., 2020).

a modified Archie's law  $f_p = 1.5\rho_f/\rho$ , which is confirmed by numerical calculations for media containing cubic or globular high-resistance inclusions along which the fluid is distributed. Laboratory studies showed that a twofold decrease in the content of the fluid fractions  $f_p$  bound in filaments, if their concentration is the same, leads to an 8- to 10-fold increase in the resistivity of rock blocks (Shimoyuku et al., 2014). The dependence of  $\rho_f$  of the mineralized water solution on temperature and pressure was taken from the paper (Physical properties..., 1984).

The mineralization of groundwater in the North Caucasus varies from the first few grams to several hundred grams per liter (Lavrushin, 2012). When we calculated the electrical conductivity of the fluid, we took into account the data on its average mineralization by sodium chloride salts within: the Taman Peninsula with  $C = 16\text{--}20$  g/L, the central part of the North Caucasus with  $C = 10$  g/L, and the eastern part of the North Caucasus with  $C = 8$  g/L. At temperature  $T = 18^\circ\text{C}$  and atmospheric pressure, we have:  $\rho_f = 0.4$   $\Omega$  m,  $\rho_f = 0.6$   $\Omega$  m, and  $\rho_f = 0.8$   $\Omega$  m, respectively.

At depths of 3 and 10 km in the crust of the Taman Peninsula, the temperature is 120 and 300°C (Ershov et al., 2015). An increase in pressure and temperature with depth gives  $\rho_f$  at:  $H = 3$  km ( $T = 120^\circ\text{C}$ )— $\rho_f = 0.13$   $\Omega$  m, 5 km ( $T = 200^\circ\text{C}$ )— $\rho_f = 0.1$   $\Omega$  m and by 10 km ( $T = 300^\circ\text{C}$ )  $\rho_f = 0.05$   $\Omega$  m. When estimating the content of bound fluid fractions, it is assumed that for depths of 3–5 km  $\rho_f = 0.1$   $\Omega$  m, and for depths of 6–10 km— $\rho_f = 0.07$   $\Omega$  m.

For the central part of the North Caucasus, the temperature reaches:  $T = 100\text{--}150^\circ\text{C}$  at depths of 5–6 km,  $T = 200\text{--}300^\circ\text{C}$  at depths of 8–10 km,  $T = 500\text{--}600^\circ\text{C}$  at depths of 15–20 km, and  $T = 600\text{--}800^\circ\text{C}$  at a depth of 30 km, which results in:  $\rho_f = 0.2$   $\Omega$  m,  $\rho_f = 0.1\text{--}0.08$   $\Omega$  m,  $\rho_f = 0.05\text{--}0.06$   $\Omega$  m, and  $\rho_f = 0.04$   $\Omega$  m, respectively. Similar estimates of  $\rho_f$  were also obtained for the eastern part of the North Caucasus (Belyavsky, 2022).

The content of all fluid fractions  $f_v$  in low-velocity crustal blocks was estimated by means of the time average equation of (Wyllie et al., 1956):  $f_v = (V_f/V_p)(V_o - V_p)/(V_o - V_f)$ , where  $V_f = 1.7$  km/s is the velocity of longitudinal waves in water;  $V_p$  is the velocity in the block with water fluids;  $V_o$  is the velocity in the dehydrated crustal block. Distribution of the relative anomalies of longitudinal wave velocities on the ECWM profiles that are close to or coincide with Pr. V, Pr. XII, Pr. X, and Pr. IX are taken from the papers by (Shempelev et al., 2020; Belyavsky et al., 2007). The content of  $f_v$  and its bound water fractions  $f_p$  in the crust of the North Caucasus marginal massif and its adjacent areas is given in Table, which shows the distribution of the relative velocity deficit  $\Delta V_p/V_o$  of lon-

gitudinal seismic waves (second column) and the resistivity  $\rho_{in}(X_{in}, Y_{in}, Z_{in})$  (fifth column).

The resulting distribution of bound fluid fractions  $f_p$  and the depth of their concentration are shown in Fig. 11. Within the Mineralnye Vody outcrop and the North Caucasus marginal massif, deeper than 5–10 km,  $f_p$  is close to the  $f_v$  values or lower (Table 1). Laboratory studies showed that an increase in  $f_v$  relative to  $f_p$  is associated with the adsorption of some NaCl ions on the capillary walls (Shimoyuku et al., 2014).

The fact that  $f_p$  exceeds  $f_v$  under o.p.: 25–52 (Pr. V), 207–208 (Pr. X), 108 (Pr. XII) can be explained by a higher content of sodium chloride salts in the fluid than assumed in the estimation of  $f_p$  or by the manifestation of the equivalence principle in the estimation of  $\rho_{in}$ , when the change of the conductor thickness is proportional to its resistivity. For example, in the test model (Fig. 3a), at the integral conductivity  $S_i$  under i.p. 36–41 of the block with  $S_i = 1700\text{--}2000$  S and its  $\rho_t = 10$   $\Omega$  m, the reduction in the obtained  $\rho_{in}$  to 3–5  $\Omega$  m and the anomaly thickness to  $h_{in} = 5000$  m (Fig. 3b) leads to an increase in the estimated  $f_p$ . The increase in the thickness of the conductivity anomaly  $h_{in}$  (i.p. 30–36, Fig. 4d) to 3–4 km compared to the model block with  $h_t = 0.5$  km (Fig. 4a), with an increase in its  $\rho_{in}$  to 5–10  $\Omega$  m ( $\rho_t = 1$   $\Omega$  m) leads to an apparent decrease in its  $f_p$ .

Introducing additional constraints, e.g. from seismic data, on the parameters of the conducting blocks allows a more reliable determination of  $\rho_{in}(X_{in}, Y_{in}, Z_{in})$  and  $f_p$ , as does making corrections to the scale of possible deviations of  $\rho_{in}$  based on the  $\delta_{xy}$ ,  $\delta_{yx}$  inversion errors. The above assumption that fluid mineralization is constant in the parts of the North Caucasus allows us to make changes in the  $f_p$  estimates shown in Fig. 11 proportional to actual changes in the values of its mineralization and Archie's law.

## RESULTS

1. Within the deep faults and suture zones intersecting the Mineralnye Vody outcrop and the North Caucasus marginal massif, the maximum content of fluid with  $f_p = 2\text{--}9\%$  is concentrated at depths of 2–15 km (Figs. 10c, 11) in the zones:

– The fault intersections: the Cherkessk fault and the Armavir–Nevinnomyssk fault (o.p. 206–208, Pr. X), the Naguta fault and the Naguta–Lysaya Gora fault (o.p. 98–116, Pr. V), the Naguta–Lysaya Gora fault and the eastern boundary of the Elbrus–Mineralnye Vody zone (Pr. XII, o.p. 113–117, o.p. 108).

– The junctions of the North Caucasus massif with the East Kuban (Pr. IV, o.p. 6–8) and Terek–Caspian

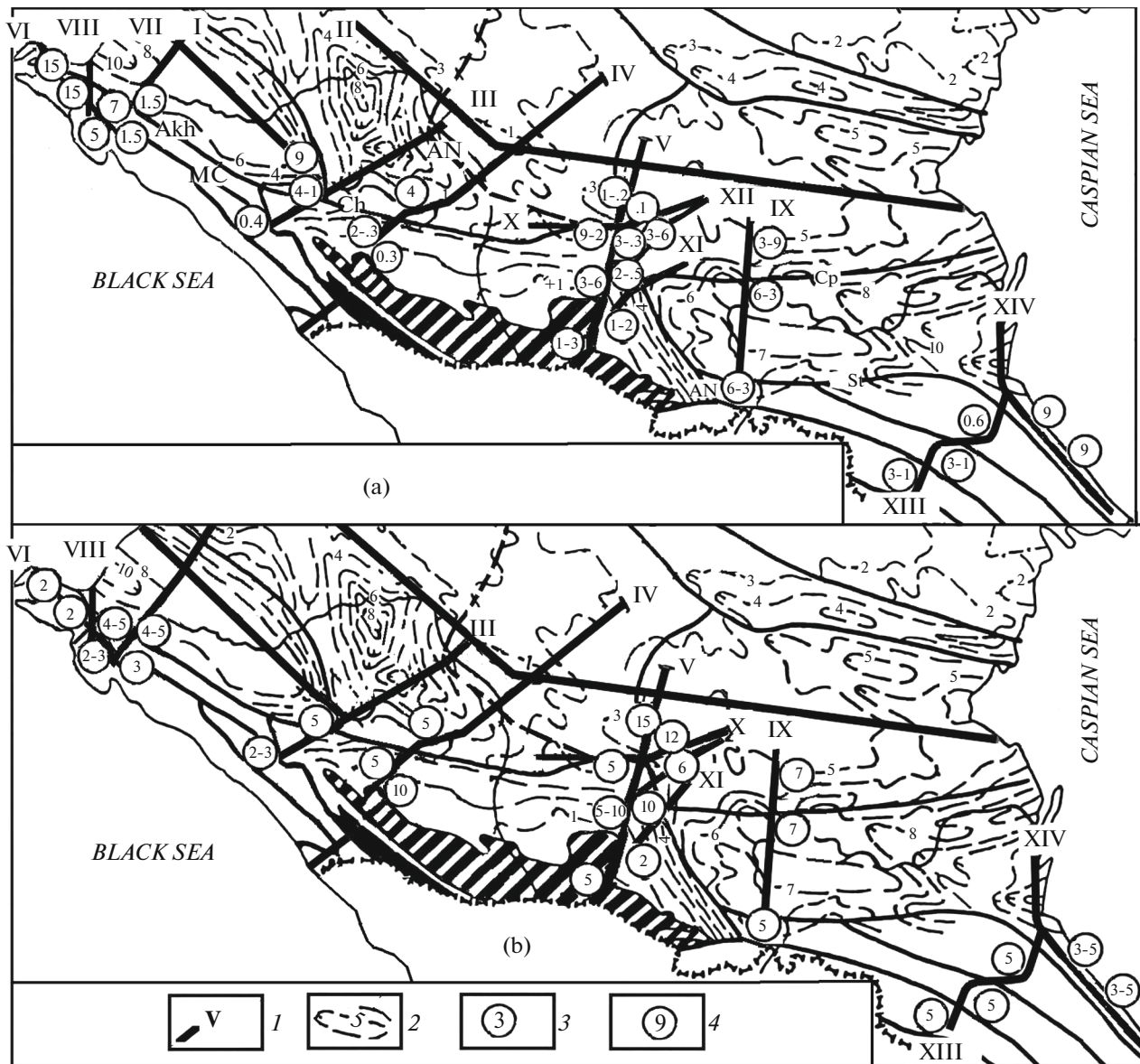


**Fig. 11.** Distribution of bound fluid fractions  $f_p$  (%) in the North Caucasus region: 1—MTS profiles, 2—depth to the basement; 3—fluid fraction (a); 4—depth to the zones of increased  $f_p$  content (b).

(Pr. XI, o.p. 302–304) troughs along the Cherkessk and Mineralnye Vody faults.

— The overthrust from 15 to 5 km from the Arma-  
vir–Nevinnomyssk fault to the Tyrnauz fault (Pr. V,  
o.p. 52–25) and the Elbrus volcanic chamber  
(Figs. 3b, 10, 11).

The high conductivity of crustal blocks correlates  
with domains of reduced velocities of seismic waves  
up to 5% (Table 1) or/and their increased absorption  
(Figs. 3, 6, 9). These facts are explained by the  
high fluid content in the decompacted planes of the  
thrust of the Scythian plate crust over the southern  
microplate (Shempelev et al., 2005), activation of deep

faults, and the “fluid-bearing vent of the Elbrus vol-  
cano” (Shempelev et al., 2020).

2. In the chambers of mud volcanoes of the Taman  
trough (Pr. VI, o.p. 41, 44, 47, and 52–55, Fig. 1),  
at the intersections of the Main Caucasian and Akhtyr  
deep faults with the regional (Dzhiginka and Anapa)  
ones, which separate the folded structures of the Cau-  
casus from the Taman trough (Pr. VI, o.p. 74–75;  
Pr. VII, o.p. 8–11) and in the eastern part of the  
Indol–Kuban trough (Pr. VII, o.p. 53) the content of the  
fluid water fraction  $f_p = 5–20\%$  with  $\rho_{in} = 1–4 \Omega \text{ m}$   
(Figs. 10, 11). These regions are associated with the  
position of the domains of increased absorption of

**Table 1.** Distribution of the fluid water fraction

MTS Pr. (ECWM Pr.)	$\Delta V_p/V_o$ in %; $f_v$ , in %; $V_o = 6.4$ km/s to $H = 20$ km and $V_o = 6.8$ km/s for $H > 20$ km	$H_p$ —depths to the top and bottom of the low-velocity block (MTS o.p.)	$T$ , °C; structures—shear zones, faults	$\rho_{in}$ ( $\Omega$ m) of the block, its $H_{in}$ (km) and the portion of the fluid water fraction $f_p$ in % of the block volume
Pr. X	1) 3–4%, $f_v = 1–1.4\%$	1) $H_p = 12–25$ km, (207–208)	1) $T = 100–250^\circ\text{C}$ , Cherkessk fault, Nalchik–Mineralnye Vody zone	1) $\rho_{in} = 10–3$ , $H_{in} = 4$ km, $f_p = 2–8\%$ , $f_p = 1.5–4\%$ (10 km)
	2) 2–4%, $f_v = 0.7–1.4\%$	2) $H_p = 8–25$ km, (212–214)	2) $T = 100–400^\circ\text{C}$ , Naguta–Lysaya Gora fault	2) $\rho_{in} = 100–200$ , $H_{in} = 5–20$ , $f_p \approx 0.1\%$
Pr. V	1) 10–7%, $f_v = 5–3\%$	1) $H_p = 5–35$ km, (1–3)	1) $T = 100–400^\circ\text{C}$ , Elbrus volcano	1) $\rho_{in} = 5–10$ , $H_{in} = 7–12$ km, $f_p = 1.5–3\%$
	2) 3–5%, $f_v = 1–2\%$	2) $H_p = 5–15$ km, (25–52), 40–50, (60–100)	2) $T = 150–400^\circ\text{C}$	2) $\rho_{in} = 3–5$ , $H_{in} = 5–10$ km, $f_p = 6–3\%$
	3) 2–4%, $f_v = 0.7–1.4\%$	3) $H_p = 15–40$ km, (80–116)	3) $T = 200–600^\circ\text{C}$ , Nalchik–Mineralnye Vody zone, Mineralnye Vody fault	3) $\rho_{in} = 10–50$ , $H_{in} = 15$ km, $f_p = 1–0.2\%$ ; $H_{in} = 30$ , $f_p = 0.5–0.1\%$
Pr. XII	1) 3–6%, $f_v = 1–2\%$	1) $H_p = 5–25$ , (117–113)	1) $T = 200–600^\circ\text{C}$ , Mineralnye Vody fault, boundary of the Elbrus–Mineralnye Vody zone	1) $\rho_{in} = 10–30$ , $H_{in} = 10$ km, $f_p = 1.5–0.5\%$ , $f_p = 0.45–0.15\%$ , $H_{in} = 30$
	2) 2–4%, $f_v = 0.7–1.3\%$	2) $H_p = 5–20$ km, (113–109)	2) $T = 100–200^\circ\text{C}$ , Elbrus–Mineralnye Vody fault and Naguta–Lysaya Gora fault	2) $\rho_{in} = 10–30$ , $f_p = 1.5–0.3\%$ , $H_{in} = 10$ km, $f_p = 3–0.6\%$ , $H_{in} = 5$ km
	3) 2–4%, $f_v = 0.7–1.3\%$	3) $H_p = 5–15$ km, (108)	3) $H = 4–10$ km, $T = 100–200^\circ\text{C}$ , Elbrus–Mineralnye Vody zone	3) $\rho_{in} = 2–5$ , $H_{in} = 7–9$ km, $f_p = 3–6\%$
Pr. IX	4.8%, $f_v = 2.7\%$	$H_p = 8–20$ km, (26, 27)	$T = 150–200^\circ\text{C}$ , Middle fault	$\rho_{in} = 4–5$ , $f_p = 6–3\%$ , $H = 7–9$ km

transverse converted waves confined to the fluid inflow channels (<sup>2</sup>Rogozhin et al., 2019). Thus, in the area of the Akhtyr fault, which bounds the Greater Caucasus in the northwest, their attenuation is three times greater than the reference values.

In the northeast of the Novorossiysk folded zone near the Akhtyr and Main Caucasian deep faults,  $f_p$

decreases to 1–2%, and under Pr. III (o.p. 2–4, 17–23) it also decreases to  $f_p = 0.4–1.5\%$  ( $\rho_{in} = 50–10 \Omega$  m) at depths of  $Z_{in} = 4–10$  km (Figs. 10b, 11) at the junction of the Greater Caucasus and Indol–Kuban trough structures (Pr. I, o.p. 2, 4–10) (Belyavsky, 2023). These blocks are also characterized by lower attenuation of transverse waves (Rogozhin et al., 2015) in the band of the Scythian plate subduction beneath

the Greater Caucasus (Zolotov et al., 2001). Within these structures, from the Anapa fault to the Novorossiysk folded zone, earthquakes of magnitude  $M > 5$  occur (Stogny, G.A. and Stogny, V.V., 2019).

3. In the eastern part of the North Caucasus, under the folded structures of the Lateral Range, the Agvali monocline, and Limestone Dagestan (Pr. XIII), at depths of 5–8 km, blocks with  $f_p = 3–1\%$  ( $\rho_{in} = 10–30 \Omega \text{ m}$ ) (Belyavsky, 2022) extend from the Main Range of the Greater Caucasus to the Terek–Caspian trough (Fig. 11). Within the belts separating the main high–resistance structures of the Eastern Caucasus, anomalies of elevated  $f_p$  sink northward from a depth of 1 to 5 km beneath the Lateral Range, the Agvali monocline, and Limestone Dagestan. The position of these zones of fluid saturation is associated with the junction of the Terek–Caspian trough and the folded structures of the Eastern Caucasus (Magometov, 2010). In it, the Dagestan wedge (Fig. 1) consists of a system of fractured thrusts over the Paleocene–Eocene sediments along which fluid can flow, creating a system of conducting structures.

In the Terek–Caspian trough (Pr. IX), at depths of 5–7 km under the Northern frontal overthrust of the Eastern Caucasus (o.p. 1) and in the vicinity of the Middle fault (o.p. 27), which separates the Terek–Kuma depression and the Terek–Caspian trough,  $f_p = 6–3\%$  (Fig. 11). The first block of fluid saturation is associated with the southern dip of the Greater Caucasus structures thrust over the Terek–Caspian trough (Belov et al., 1990). It correlates with the anomaly of increased absorption of VS wave velocities up to 3–4 dB found at depths of 15–25 km (Rogozhin et al., 2019), which is explained by the “advective penetration of light low–density material into the crust.” The second zone of fluid saturation correlates with the position of the lower velocity block with  $V = 5.9 \text{ km/s}$ , at the average crustal velocity  $V = 6.2 \text{ km/s}$  (Krasnopevtseva, 1978), which corresponds to  $f_v \approx 3\%$ , close to that estimated by  $f_p$ . In the eastern part of the Terek–Caspian trough (Pr. XIV), under latitudinal faults at depths of 3–8 km, conductivity anomalies with  $f_p = 9\%$  were found (Belyavsky, 2022).

4. In the central sector of the North Caucasus, the conducting region under the Mineralnye Vody outcrop and marginal massif includes the Naguta–Lysaya Gora and Mineralnye Vody shear structures (Fig. 3c). Together with the Armavir–Nevinnomyssk fault, they correlate with the location of three bands of increased seismicity (Figs. 9, 10c) (Gabsatarova et al., 2020). The Northern frontal overthrust ( $f_p = 3–6\%$ ), adjacent to the Vladikavkaz fault (o.p. 3, Pr. IX), is surrounded by a seismic lineament with magnitudes of possible earthquakes up to  $M_{max} = 6.5–7.1$  (Asmanov et al., 2013) (Fig. 1). This concentration of earthquake sources reflects “... the migration of deep fluid flows

along the beds with reduced velocities of longitudinal waves, which are located parallel to the high–speed block” (Krasnopevtseva and Kuzin, 2009). Within the Dagestan wedge and the Terek–Caspian trough areas adjacent to the wedge, the observed high fluid saturation (Fig. 11) reduces the viscosity and stability of the activated crustal zones, which is manifested in the concentration of epicenters of lithospheric earthquakes.

It can be said that the increased conductivity (ionic type) of the crust associated with its physical and chemical properties makes it possible to solve the problems of geodynamics and seismic activity.

#### ACKNOWLEDGMENTS

I am grateful to the organizations that provided the primary electrical survey material, Electromagnetic Research Center LLC and Severo-Zapad LLC. The paper examines the seismic data obtained with the earthquake converted wave method (ECWM) in 1990–2006 by the GEON Center.<sup>1</sup>

#### CONFLICT OF INTEREST

The author declares that he has no conflicts of interest.

#### REFERENCES

- Asmanov, O.A., Adilov, Z.A., and Daniyalov, M.G., Seismic material analysis for medium seismic zoning of Dagestan, *Tr. Inst. Geol. Dagest. Nauchn. Tsentra RAN*, 2013, no. 62, pp. 218–222.
- Atlas kart Severnogo Kavkaza: tektonicheskaya karta Severnogo Kavkaza. Masshtab 1 : 1000000* (Atlas of North Caucasus Maps: Tectonic Map of the North Caucasus, scale 1 : 1000000), Prutskii, N.I., Ed., Essentuki: Severo-Kavkazskii regional'nyi geologicheskii tsentr MPR Rossii, 1998.
- Belov, A.A., Burtman, V.S., Zinkevich, V.P., Baranov, G.I., Dobrzhinetskaya, L.F., Dotduev, S.I., Zlobin, V.L., Knipper, A.L., Kurenkov, S.A., Lobkovskii, L.I., Luk'yanov, A.V., Mazarovich, A.O., Markov, M.S., Perfil'ev, A.S., Pushcharovskii, Yu.M., et al., *Tektonicheskaya rassloennost' litosfery i regional'nye geologicheskie issledovaniya (Tectonic Delamination of the Lithosphere and Regional Geological Investigations)*, Pushcharovskii, Yu.M., Trifinov, V.G., and Nikitina, T.A., Eds., Moscow: Nauka, 1990.
- Belyavskii, V.V., *Geoelektricheskaya model' tektonosfery Severo-Kavkazskogo regiona* (Goelectric Model of the North Caucasus Tectonosphere), Moscow: GERS, 2007.
- Belyavskii, V.V., Goelectric model of the Eastern Caucasus (three-dimensional inversion), *Geofizika*, 2022, no. 2, pp. 64–69.
- Belyavskii, V.V., Seismotectonic model of the Northwestern Caucasus: three-dimensional inversion, *Fiz. Zemli*, 2023, no. 2, pp. 78–93.
- Belyavskii, V.V., Egorkin, A.V., Rakitov, V.A., Solodilov, L.N., and Yakovlev, A.G., Some results of applying methods of natural electromagnetic and seismic fields in the North Caucasus, *Izv., Phys. Solid Earth*, 2007, vol. 43, no. 4, pp. 268–277.



- Berdichevsky, M.N. and Dmitriev, V.I., *Models and Methods of Magnetotellurics*, Berlin: Springer, 2008.
- Brown, G.C. and Musset, A.E., *The Inaccessible Earth*, London: George Allen and Unwin, 1981.
- Bulin, N.K. and Egorkin, A.V., *Regional'nyi prognoz nefetegazonosnosti nedr po glubinnym seismicheskim kriteriyam* (Regional Prediction of Oil and Gas Content on the Basis of Deep Seismic Criteria), Moscow: Tsentr GEON, 2000.
- Counil, J.L., le Mouel, J.L., and Menvielle, M., Associate and conjugate directions concepts in magnetotellurics, *Ann. Geophys.*, 1986, vol. 4B, no. 2, pp. 115–130.
- Druskin, V. and Knizhnerman, L., Spectral approach to solving three-dimensional Maxwell's diffusion equations in the time and frequency domains, *Radio Sci.*, 1994, vol. 29, no. 4, pp. 937–953.
- Ershov, V.V., Sobisevich, A.L., and Puzich, I.N., Deep underground structure of mud volcanoes in Taman according to experimental field studies and mathematical modeling, *Geofiz. Issled.*, 2015, vol. 16, no. 2, pp. 69–76.
- Fizicheskie svoystva gornykh porod i poleznykh iskopaemykh (petrofizika). Spravochnik geofizika* (Physical Properties of Rocks and Minerals (Petrophysics). *Geophysics Handbook*), 2nd ed., Dortman, N.B., Ed., Moscow: Nedra, 1984.
- Gabsatarova, I.P., Koroletski, L.N., Ivanova, L.E., and Selivanova, E.A., Zavetnoye earthquake on May 2, 2012 with  $K_p = 11.2$ ,  $M_{w\text{per}} = 4.3$ ,  $I_0^p = 5$  and Vorovskoleskaya—II earthquake on December 15, 2012 with  $K_p = 10.8$ ,  $M_{w\text{per}} = 4.2$ ,  $I_0^p = 4$  (Stavropol region), *Zemletryaseniya Sev. Evrazii*, 2018, no. 21 (2012), pp. 323–331.
- Ivanov, P.V. and Pushkarev, P.Yu., Three-dimensional inversion of the single-profile magnetotelluric data, *Izv., Phys. Solid Earth*, 2012, vol. 48, no. 11–12, pp. 871–876.
- Kiyan, D., Jones, A.G., and Vozar, J., The inability of magnetotelluric off-diagonal impedance tensor elements to sense oblique conductors in three-dimensional inversion, *Geophys. J. Int.*, 2014, vol. 196, no. 3, pp. 1351–1364.
- Krasnopenvtseva, G.V., The deep structure of the Caucasus, in *Stroenie zemnoi kory i verkhnei mantii Tsentral'noi i Vostochnoi Evropy* (The Structure of the Earth's Crust and the Upper Mantle of Central and Eastern Europe), Sollogub, V.B., Guterkh, A., and Prosen, D., Eds., Kiev: Naukova dumka, 1978, pp. 190–199.
- Krasnopenvtseva, G.V. and Kuzin, A.M., Comprehensive seismic interpretation of DSS data (longitudinal waves) based on the Volgograd–Nakhichevan profile, in *Razlomoobrazovanie i seismichnost' v litosfere: tektonicheskie kontseptsii i sledstviya: Materialy Vseross. Soveshchaniya* (Faulting and Seismicity in the Lithosphere: Tectonophysical Concepts and Consequences: Proc. of the All-Russ. Conf.), 18–21 August 2009, Irkutsk, Irkutsk: IZK SO RAN, 2009, vol. 1, pp. 61–63.
- Kurbanov, M.K., *Geotermal'nue i gidromineral'nue resursy Vostochnogo Kavkaza i Predkavkaz'ya* (Geothermal and Hydromineral Resources of the Eastern Caucasus and Ciscaucasia), Kamilov, I.K. and Polyak, B.G., Eds., Moscow: Nauka, 2001.
- Lavrushin, V.Yu., *Podzemnye flyuidy Bol'shogo Kavkaza i ego obramleniya* (Subsurface Fluids of the Greater Caucasus and Its Surrounding), vol. 599, Polyak, B.G., Ed., Tr. GIN RAN, Moscow: GEOS, 2012.
- Levin, L.E. and Kondorskaya, N.V., Seismicity of the central Mediterranean belt of Eurasia in relation to the development of the oil and gas complex, *Razved. Okhr. Nedr*, 1998, no. 2, pp. 28–31.
- Lukk, A.A. and Shevchenko, V.I., Seismicity, tectonics, and GPS geodynamics of the Caucasus, *Izv., Phys. Solid Earth*, 2019, vol. 55, no. 4, pp. 626–648.
- Magomedov, R.A., Geodynamic regime of the region of the Dagestan wedge in the Alpine cycle of the Eastern Caucasus, *Tr. Inst. Geol. Dagest. Nauchn. Tsentra RAN*, 2010, no. 56, pp. 66–79.
- Miensopust, M.P., Queralt, P., Jones, A.G., and the 3D MT modelers Collab., Magnetotelluric 3D inversion—review of two successful workshops on forward and inversion code testing and comparison, *Geophys. J. Int.*, 2013, vol. 193, no. 3, pp. 1216–1238.
- Milanovskii, E.E., Rastsvetaev, L.M., Kukhmazov, S.U., Birman, A.S., Kudrin, N.N., Simako, V.G., and Tveritinoва, T.Yu., Recent geodynamics of the Elbrus–Mineralovodsk region of the North Caucasus, in *Geodinamika Kavkaza* (The Caucasus Geodynamics), Belov, A.A. and Sattian, M.A., Eds., Moscow: Nauka, 1989, pp. 99–105.
- Rogozhin, E.A., Gorbatikov, A.V., Stepanova, M.Yu., Ovsyuchenko, A.N., Andreeva, N.V., and Kharazova, Yu.V., The structural framework and recent geodynamics of the Greater Caucasus meganticlinorium in the light of new data on its deep structure, *Geotectonics*, 2015, vol. 49, no. 2, pp. 123–134.
- Rogozhin, E.A., Milyukov, V.K., Mironov, A.P., Ovsyuchenko, A.N., Gorbatikov, A.V., Andreeva, N.V., Lukashova, R.N., Drobyshev, V.I., and Khubaev, Kh.M., Characteristics of the modern horizontal movements in the zones of the strong and moderate earthquakes in the beginning of the XXI century in the central sector of the Greater Caucasus according to GPS-observations and their connection with the Earth's crust neotectonics and deep structure, *Izv., Atmos., Ocean., Phys.*, 2019, vol. 55, no. 7, pp. 759–769.
- Rogozhin, E.A., Gorbatikov, A.V., Kharazova, Yu.V., Stepanova, M.Yu., Chen, J., Ovsyuchenko, A.N., Lar'kov, A.S., and Sysolin, A.I., Deep structure of the Anapa flexural-rupture zone, Western Caucasus, *Geotectonics*, 2019, vol. 53, no. 5, pp. 541–547.
- Shankland, T.J. and Waff, H.S., Partial melting and electrical conductivity anomalies in the upper mantle, *J. Geophys. Res.*, [Solid Earth Planets], 1977, vol. 82, no. 33, pp. 5409–5417.
- Shempelev, A.G., P'yankov, V.Ya., Lygin, V.A., Kukhmazov, S.U., and Morozov, A.G., Results of geophysical studies along the near-Elbrus profile (Elbrus volcano—Caucasian Mineral Waters, *Reg. Geol. Metallog.*, 2005, no. 25, pp. 178–185.
- Shempelev, A.G., Zaalishvili, V.B., Chotchaev, Kh.O., Shamanovskaya, S.P., and Rogozhin, E.A., Tectonic fragmentation and geodynamic regime of Elbrus and Kazbek volcanoes (Central Caucasus, Russia): results of the deep geophysical research, *Geotectonics*, 2020, vol. 54, no. 5, pp. 652–664.
- Shimoyuku, A., Yoshino, T., Yamazaki, D., Electrical conductivity of brine-bearing quartzite at 1 GPa: implications for fluid content and salinity of the crust, *Earth, Planets Space*, 2014, vol. 66, Article ID 2. <https://doi.org/10.1186/1880-5981-66-2>



- Siripunvaraporn, W., Egbert, G., Lenbury, Y., and Uyeshima, M., Three-dimensional magnetotelluric inversion: data-space method, *Phys. Earth Planet. Inter.*, 2005, vol. 150, no. 1–3, pp. 3–14.  
<https://doi.org/10.1016/j.1365-246X.2005.02527>
- Siripunvaraporn, W., Egbert, G., Lenbury, Y., and Uyeshima, M., Interpretation of two-dimensional magnetotelluric profile data with three-dimensional inversion: synthetic examples, *Geophys. J. Int.*, 2005, vol. 160, no. 3, pp. 804–814.  
<https://doi.org/10.1111/j.1365-246X.2005.02527>
- Sobisevich, A.L., Laverova, N.I., Sobisevich, L.E., Mikadze, E.I., and Ovsyuchenko, A.N., *Seismoaktivnye flyuidomagmaticheskie sistemy Severnogo Kavkaza (Seismoactive and Fluid-Magmatic Systems of Northern Caucasus)*, Laverov, N.P., Ed., Moscow: IFZ RAN, 2005.
- Stongy, G.A. and Stongy, V.V., Seismotectonic model of the Northwest Caucasus: geological-geophysical aspect, *Izv. Phys. Solid Earth*, 2019, vol. 55, no. 4, pp. 649–656.
- Varentsov, I.M., A general approach to the magnetotelluric data inversion in a piecewise–continuous medium, *Fiz. Zemli*, 2002, no. 11, pp. 11–33.
- Voblikov, B.G. and Lopatin, A.F., Tectonic structure of Paleozoic deposits in the central and eastern Ciscaucasia, in *Tektonika i geodinamika (Tectonics and Geodynamics)*, Stavropol': SevKavGTU, 2002, pp. 87–108.
- Wyllie, M.R.J., Gregory, A.R., and Gardner, L.W., Elastic wave velocities in heterogeneous and porous media, *Geophysics*, 1956, vol. 21, no. 1, pp. 41–70.
- Zolotov, E.E., Kadurin, I.N., Kadurina, L.S., Nedyad'ko, V.V., Rakitov, V.A., Rogozhin, E.A., and Lyashenko, L.L., New data on the depth structure of the Earth's crust and seismicity of the Western Caucasus, in *Geofizika XXI stoletiya: Sb. Tr. Tre'tikh geofizicheskikh chtenii im. V.V. Fedynskogo (Geophysics of XXI Century: Collection Proc. 3d Readings on Geophysics in Memory of V.V. Fedynsky)*, Solodilov, L.N., Ed., Moscow: Nauchnyi Mir, 2001, pp. 85–89.
- Zonov, S.V., Zraiskii, G.P., and Balashov, V.I., Effect of thermally–induced dilatation on the permeability of granite in cases in which the lithostatic pressure slightly exceeds the fluid pressure, *Dokl. Akad. Nauk SSSR*, 1989, vol. 307, no. 1, pp. 191–195.